RICHTMYER – MESHKOV INSTABILITY

IN REACTIVE MIXTURES

By

MADHURI UNGARALA

Presented to the Faculty of the Graduate School of

The University of Texas at Arlington in Partial Fulfillment

Of the Requirements

For the Degree of

MASTER OF SCIENCE IN AEROSPACE ENGENEERING

THE UNIVERSITY OF TEXAS AT ARLINGTON

May 2010

TO MY MOM, DAD, BROTHER AND FRIENDS

ACKNOWLEDGEMETS

I feel grateful to have this opportunity to express my sincere appreciation to all of the people who have supported me during my masters.

First and foremost, I would like to express my deepest gratitude to my advisor Dr. Luca Massa for his endless support and encouragement throughout my research work. It is my privilege to work with him on my research work which enabled me to gain a good knowledge in the subject. His valuable suggestions, comments and motivational talk inspired me to work hard and achieve my goal.

My sincere thanks to my committee members, Dr. Frank Lu and Dr. Donald Wilson, who have allotted their precious time from their busy schedule to review my research work. I would like to thank Dr. Lu for joining me with the ARC group and updating everyone with the new research tools available, posting some very useful links and employment opportunities. I would like thank Dr. Wilson for evaluating my performance in the graduate seminar course and providing me with valuable suggestions.

I am indebted to my parents and brother for their endless love and encouragement given to me in every situation I faced being far away from them. I would always be thankful to Suneel Jinnala, Raghu Ram Ghandikota, Kishore Nekkanti and Hari Nagarajan for understanding my research interests and introducing me to Dr. Massa. Sincere thanks to my manager Ms. Kristina Clark, (Office of Students with Disabilities) for being a great person and boosting up my confidence with her encouragement. Also, I would like to thank my best friends Vijya Yalamanchili and Divya Praturi who always keeps me smiling and constantly encourages me to succeed in my life. Life at UTA wouldn't have been so peaceful and easy without my roommates Ramya Somuri and Keerthi Parthasarathy. I would like to thank one of my close friends, Deepak Bokka for his moral support and endless help throughout my masters. My extended thanks to all my friends Poornima Mynampati, Priyam Patel, Naveen Reddy, Dinesh Varaprasad, Tej Kiran Pakyala, Divakar Kaluvagunta, Abhishek Kunchala and Justin Jones for being with me as a family and encouraging me all through my masters.

April 19, 2010

ABSTRACT

RICHTMYER-MESHKOV INSTABILITY

IN REACTIVE MIXTURES

Madhuri Ungarala, MS

The University of Texas at Arlington, 2010

Supervising Professor: Dr. Luca Massa

This research analyzes the effect of reactivity on the Richtmyer-Meshkov instability with particular emphasis on the velocity and wave number scaling and on the effect of free detonation instability modes on the interface corrugation rate. This analysis is performed by solving numerically for the first order perturbation generated by the shock-induced acceleration of an initially corrugated interface.

The objective of this research is to analyze the effect of mixture reactivity on the process supported by a shock sweeping across a corrugated interface from high density to low density fluid. This scenario is antithetical to the classical Richtmyer analysis where transmitted and reflected shock waves are generated by shock transit from low to high density mixture. A linear stability analysis of the Richtmyer-Meshkov instability supporting the detonation initiation is presented. The analysis focuses on scaling of the interface growth rate with the perturbation wave number under combustion conditions, and on the coupling between detonation front and interface instabilities. This research documents the method, numerical convergence of the solution, and results obtained assuming finite rate kinetics. The results show a profound effect of the reactivity on both the short time growth and the long time linear regime.

TABLE OF CONTENTS

LIST OF ILLUSTRATIONS

Figure Page

CHAPTER 1

INTRODUCTION

1.1 Richtmyer-Meshkov Instability

When two fluids of different density which is separated by an interface, is driven by a shock, the misalignment of pressure and density gradients gives rise to an instability of the interface, which eventually produces a turbulent mixing of fluids.

Richtmyer-Meshkov Instability (RMI), [1] refers to the instability which occurs at an impulsively accelerated interface i.e. a shock wave between two gases of different density. It differs from the Rayleigh-Taylor instability for which the acceleration at the interface is sustained, and from the Kelvin-Helmholtz instability which is due to the shear stress between the two fluids at the interface.

As the interface between the two fluids distorts, nonlinear processes eventually occur and a region of turbulence is created resulting in the mixing of the two fluids. The arrival of any additional shock wave at the interface further increases the intensity of the turbulent motions. In the case of light fluid penetrating the heavy fluid a nonlinear regime is found followed with bubbles. In the case of heavy fluid penetrating through the light fluid the formation of spikes can be observed. Turbulent mixing between the two impulsively accelerated fluids can be considered important in supersonic and hypersonic applications.

The RMI can also be used to accelerate the mixing of fuel and oxidizer in the supersonic and hypersonic engines [2]. However, the concept of interface being continuously interacted with the shock acceleration was considered first by, Markstein, [3] although the theoretical and numerical analysis of rigorous treatment of the shock-excited instability was shown by, Richtmyer [1], Martin Brouillette [3].

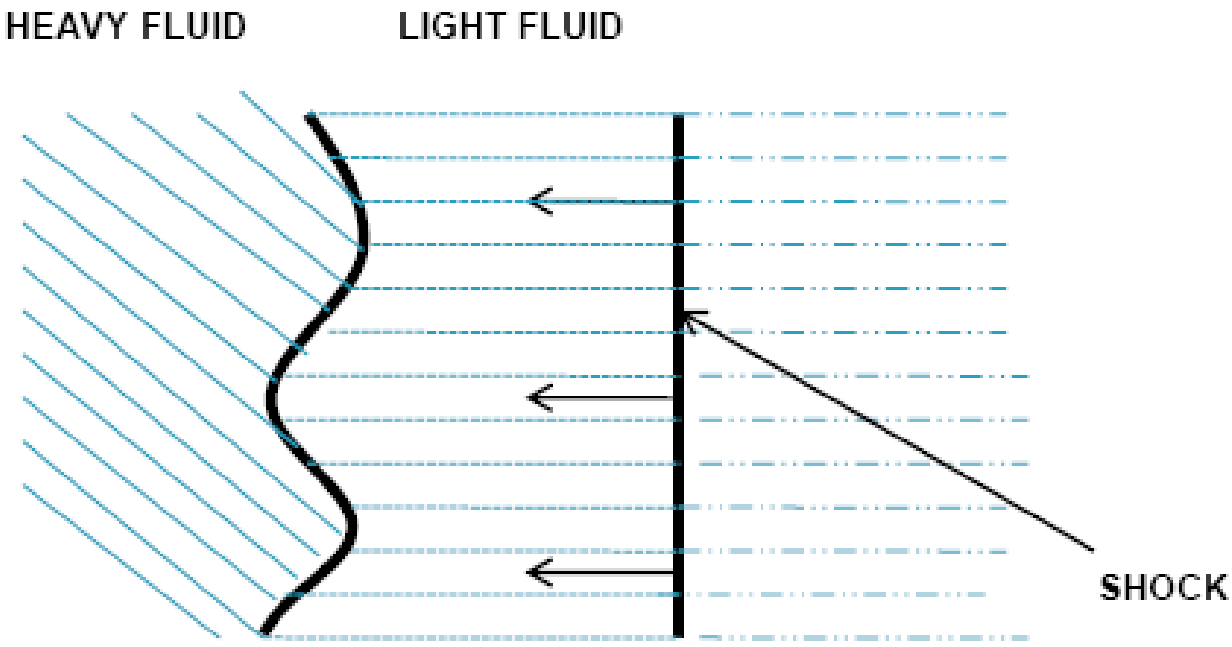

Figure 1.1: Richtmyer–Meshkov instability

The interaction of shock wave with the perturbed density interface leads to various kinds of fluid motions. RMI is referred to the shock system that is defined by a shockwave propagated along with the incident shock resulting in the supersonic instability while the reflected shock wave tends to amplify the shock system.

1.2 Applications of Richtmyer-Meshkov Instability

RMI is important in a large number of science and engineering applications. In inertial confinement fusion, RMI is important to produce ignition by impeding sufficiently powerful shockwaves which causes the mixture to compress and heat the surrounding fuel by a large set of chemical reactions to produce a nuclear fusion [4]. RMI has also been used to explain the lack of stratification of the products of supernova 1987A and is now a required ingredient in stellar evolution models [5].

The interaction of a high pressure shock wave with a subsonic flame can ignite the mixture and accelerate to supersonic speeds, hence resulting in detonating the mixture. This transition from

deflagration to detonation is named as deflagration-to-detonation transition [6]. RMI can also be used to promote mixing between fuel and oxidizer in supersonic and hypersonic air-breathing engines [7]

1.3 Introduction to the Problem

This research analyzes the role of mixture reactivity on the dynamics of the Richtmyer-Meshkov instability (reactive RMI).The phenomenon is of physical importance in the context of detonation initiation and baroclinic mixing. Previous attempts to model the RMI in reactive fluids lack a thorough examination of the mixture thermo-chemical properties on the surface deformation rate, of the induction-disturbance scaling, and of the interaction between the detonation global instability and the interface convective instability. A peculiar difference between reactive and nonreactive problems is the wave number scaling. Khoklov, analyzed the RMI resulting from flame shock interaction [6]. They note the absence of fine scale interface disturbances in burning computations, and conjecture that the flame consumes the small scales.

The Richtmyer shock problem has no geometrical length scale, so that, in the non-reactive case, the normalized growth rate of an interface disturbance scales linearly with the disturbance wave number. The premixed combustion problem that supports detonation initiation has, in its most simple form, the induction length as the length scale. The relationship between induction and disturbance wave number introduces a scaling parameter [7]. It is widely acknowledged that non-reacting shocks are stable to linear perturbations, while detonations are unstable for realistic values of the heat release. In the non-reactive Richtmyer-Meshkov problem, the interface deforms with a linear rate, while the shocks relax toward the unperturbed state with an exponential decay. In the reactive case, for a time-unstable detonation, the resonant interaction between surface deformation and detonation instability may support super-linear growth rates of interface disturbances.

Instability patterns associated with the RMI play a fundamental role in the mixing rate through the strain driven gradient steepening at the interfaces. The contribution of the initial patterns to the instantaneous mixing rate was measured to be up to 80% of the peak mixing rate, in non-reactive

measurements [8]. On the other hand, for reactive mixtures, we expect the scaling effect to alter shock induced mixing, and favor the process at selected wave numbers.

In this research we present a linear stability analysis of the RMI supporting detonation initiation. This analysis focuses on scaling of the interface growth rate with the perturbation wave number under combustion conditions, and on the coupling between the detonation front and interface instabilities. This thesis documents the method, numerical convergence of the solution, and preliminary results obtained assuming infinitely fast kinetics.

CHAPTER 2

CHEBYSHEV TAU METHOD-VALIDATION WITH EXAMPLES

2.1 Introduction to Chebyshev Polynomials

Chebyshev polynomials are of great importance in many areas of mathematics, particularly in approximation theory. They are a sequence of orthogonal polynomials which are defined recursively. There are several discretization techniques for finding the Eigen values and Eigen functions which use the finite difference technique and inverse Rayleigh iteration. Chebyshev tau-QZ method is an efficient way to find the Eigen values for a non linear partial differential equation which is a major section of the present problem. An efficient way to use the Chebyshev tau-QZ algorithm method for finding the Eigen values and Eigen functions of difficult practical problems has been discussed thoroughly in Dongarra's paper [9].

In this section, validation of the Chebyshev tau method is presented by analyzing three different problems starting from simple linear equation with single dependent variable to nonlinear partial differential equations having a vector of dependent variables.

2.2 Linear Partial Differential Equation

2.2.1 Numerical Solution

Consider the linear partial differential equation shown below

$$\frac{\partial u}{\partial t} = Ae\frac{\partial^2 u}{\partial x^2}, \tag{1}$$

where $u = u(x,t)$ and Ae =1.

The initial conditions are

$$u(x,0) = \sin[(x+1)\pi].$$

and the boundary conditions are: $u(-1,t)=0,\ u(1,t)=0.$

The equation (1) is expanded using Chebyshev expansion by writing u as a finite series of Chebyshev polynomials.

$$u=\sum_{k=0}^{N+2} u_k\, T_k(x), \tag{2}$$

where, N is the order of the maximum Chebyshev polynomial resolved in the truncation error and $T_k(x)$ is the Chebyshev polynomial of k_{th} order. Furthermore u_k is the array of Chebyshev components which is solved for,

$u_k=\begin{bmatrix} u1 \\ u2 \\ . \\ . \\ uN+2 \end{bmatrix}$, with $k=0,\dots N+2.$

The expansion takes the form

$$\frac{\partial}{\partial t}[\sum_{k=0}^{N+2} u_k\,(t)T_k(x)]=Ae\,\frac{\partial^2}{\partial^2 x}[\sum_{k=0}^{N+2} u_k\,(t)T_k(x)]\,). \tag{3}$$

Equation (1) and the boundary conditions yield a system of $(N+4)$ equations for $(N+4)$ unknowns u_i.

The boundary conditions in the Chebyshev components are

$$\sum_{k=0}^{N+2}(-1)^k u_k=0, \tag{4.a}$$

$$\sum_{k=0}^{N+2} u_k=0. \tag{4.b}$$

On differentiating equation (3) we obtain a differentiation matrix D which contains the components of Chebyshev polynomials.

$$D = \begin{pmatrix} 0 & 1 & 0 & 3 & 0 & 5 & 0 & 7 & 0 & 9 & \dots \\ 0 & 0 & 4 & 0 & 8 & 0 & 12 & 0 & 16 & 0 & \dots \\ 0 & 0 & 0 & 6 & 0 & 10 & 0 & 14 & 0 & 18 & \dots \\ 0 & 0 & 0 & 0 & 8 & 0 & 12 & 0 & 16 & 0 & \dots \\ 0 & 0 & 0 & 0 & 0 & 10 & 0 & 14 & 0 & 18 & \dots \\ \vdots & \vdots & \vdots & \vdots & \vdots & \vdots & \vdots & \vdots & \vdots & \vdots & \vdots \end{pmatrix}. \tag{4.c}$$

The expansion takes the form,

$$\frac{\partial}{\partial x}\left[\sum_{k=0}^{N+2} u_k T_k(x)\right] = \left[\sum_{k=0}^{N+2} \sum_{r=0}^{N+2} D_{kr} u_r\right] T_k. \tag{5.a}$$

In details,

$$\int_{-1}^{1} \frac{[\sum_{k=0}^{N+2} \dot{u_k}\, T_k(x) - Ae \sum_{r=0}^{N+2} \sum_{s=0}^{N+2} D_{ks}\, D_{sr} u_r] T_i(x)}{\sqrt{(1-x^2)}}\, dx = 0. \tag{5.b}$$

Note that the following are the properties of orthogonal functions in Chebyshev space. The Chebyshev polynomials of the first kind are orthogonal with respect to the measure $\sqrt{1-x^2}$.

$$\int_{-1}^{1} \frac{T_i(x) T_j(x)}{\sqrt{(1-x^2)}} dx = \begin{cases} \frac{\pi}{2}\delta_{i,j}, \\ 0 \end{cases}$$

where the Kronecker's delta is defined as δ_{ij},

$$\delta_{i,j} = \begin{cases} 1, & i = j \\ 0, & i \neq j \end{cases}.$$

Equation (5.b) is reduced by the principle of orthogonality, to the algebraic form

$$\dot{u}_k - Ae \sum_{r=0}^{N+2} \sum_{s=0}^{N+2} D_{ks}\, D_{sr} u_r \delta_{is} = 0.$$

The above equation after some algebra reduces to the ordinary differential equation

$$\dot{u}_i = Ae \sum_{k=0}^{N+2} D_{ki}^2\, u_k.$$

Given that Ae =1,

$$u_i = \sum_{k=0}^{N+2} D_{ki}^2 \, u_k. \tag{6}$$

Equation (6) is the final form. The product of *D* matrix with the matrix of unknowns, i.e. u_k, is coded in Matlab to obtain u_i.The initial condition is $u(x,0) = \sin[(x+1)\pi]$ where $\mathrm{x} = \cos\theta$, $\mathrm{x} \in (-1,1)$ and $\theta \in (\pi, 2\pi)$.

The ordinary differential equation hence obtained is solved by using the MATLAB intrinsic ode45 solver. This function implements a Runge-Kutta method with variable time step for efficient computation. The syntax for the solver-ode45 is $[T,Y] = solver\,(odefun, tspan, y0)$, where in this problem odefun is the right-hand side of equation (6), tspan is the range of integration which is taken from 0 to 0.1 in this problem, y_o is the vector of initial conditions obtained from using the algorithm discrete cosine transform by varying the angle θ in $(\pi, 2\pi)$. T is the value of the independent variable at which the solution is calculated and Y is the array of solution to the problem. Each row of the matrix Y represents the solution at the corresponding column in the vector T.

2.2.2 Exact Solution

The exact solution for the second order partial differential equation is of the form

$$u = e^{(-k^2 t)} sin(kx).$$

With the initial condition $u(x,0) = \sin[(x+1)\pi]$, the exact solution is of the form

$$u = e^{(-\pi^2 t)} \sin[(x+1)\pi]. \tag{7}$$

where t is the time step.

Figure 2.1 shows a comparison between the solution obtained numerically using Chebyshev polynomials, which is marked as O, and the exact solution is marked as X.

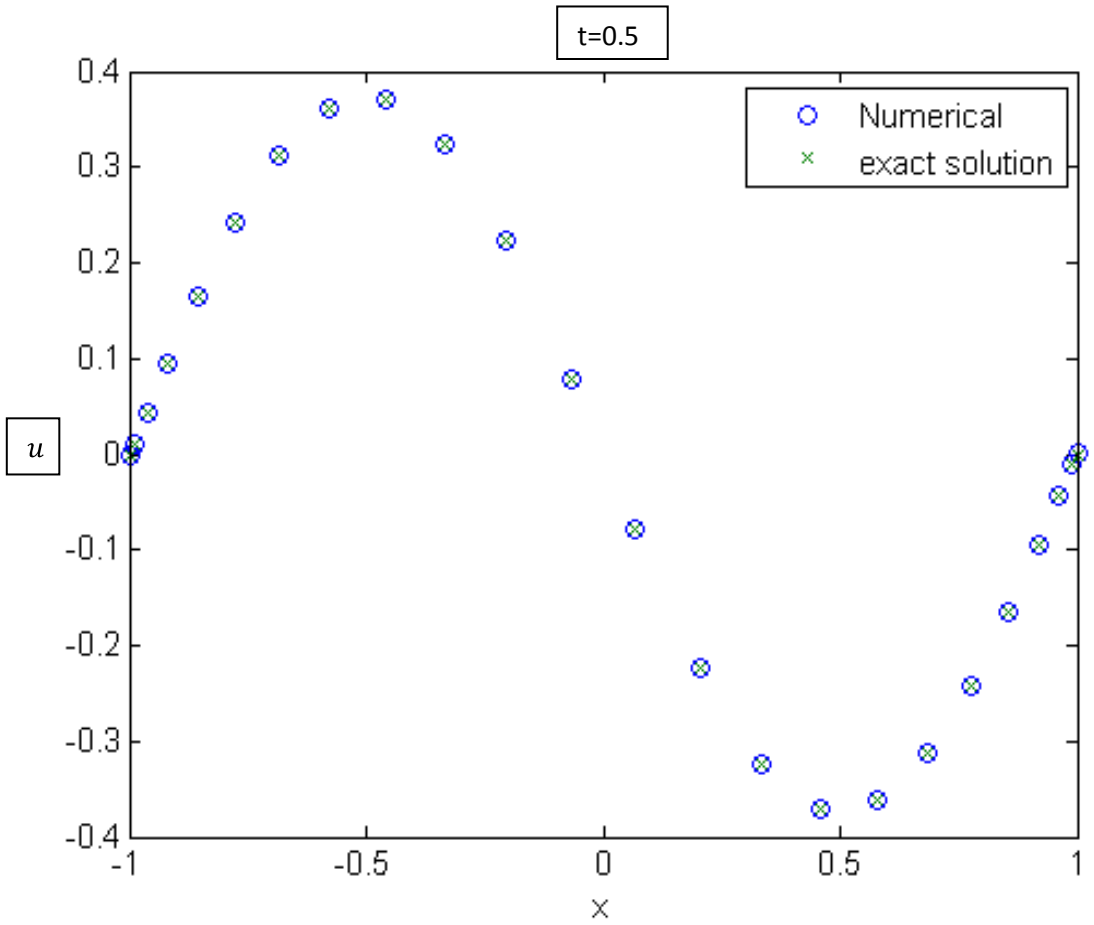

Figure 2.1: The sine curve showing the comparison between the numerical solution denoted as O and exact solution denoted as X at $t = 0.5$.

2.2.3 Error

The error between the numerical solution and the exact solution is calculated by using the relation:

E_i (Error)= Numerical Chebyshev solution- Exact solution.

The graph in Figure 2.2 shows the error to be negligible, i.e., of the order 10^{-4}.

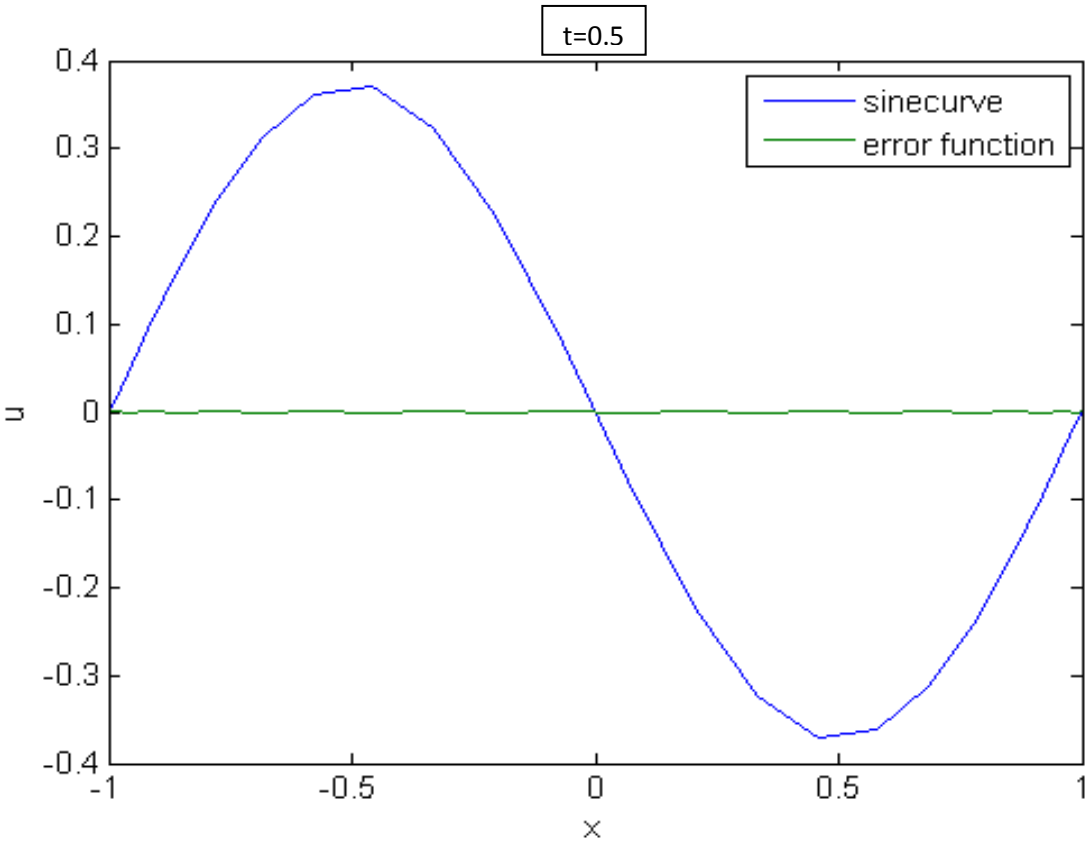

Figure 2.2: A graph showing the Chebyshev solution and the error (E_i)

2.2.4 Calculation of Error Root Mean Square

The root mean square (rms) of the error is calculated for a series of collocation points i by using the relation

$$rms=\sqrt{[\sum E_i^2]/N}. \quad (8)$$

The rms is calculated for four different polynomials namely $N = 4, 8, 12,$ and 24.

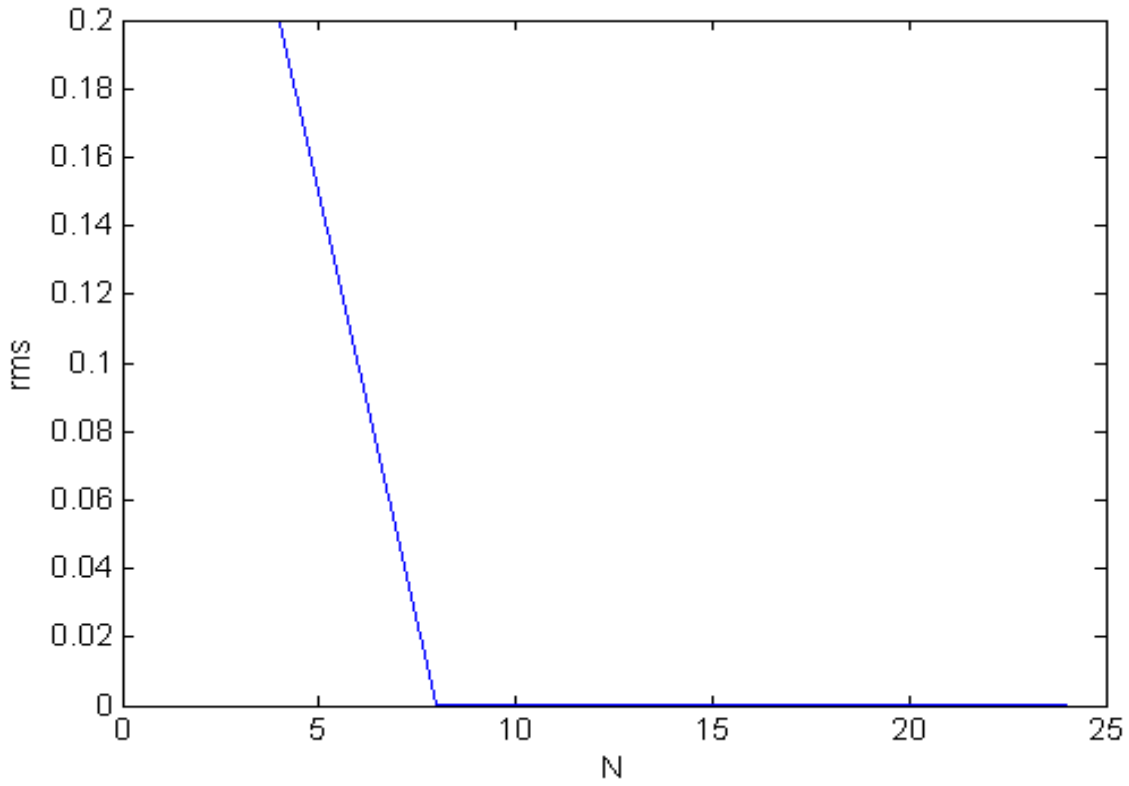

Figure 2.3: A graph showing the convergence of the solution at different N values.

2.3 Linear Vector Equation

Consider the system of equations of the form

$$\frac{\partial P}{\partial t} + \frac{A}{\delta}\frac{\partial P}{\partial x} + R = 0, \tag{9}$$

where P is a vector which contains the variables, $P = P(x,t)$ and $i = 0, \dots N+2$. In the present case

$$P = \begin{bmatrix} p \\ u \\ \rho \end{bmatrix},$$

To simplify the problem, we take $R = 0$ and $\delta = 1$.

A is a matrix which contains dependent variables as shown below:

$$A = \begin{bmatrix} u & \gamma p & 0 \\ 1/\rho & u & 0 \\ 0 & \rho & u \end{bmatrix}.$$

without loss of generality consider $u = \rho = \gamma = 1$.

The initial condition is

$$p(x, 0) = \sin[(x + 1)\pi],$$

The boundary conditions are given as

1. $p(-1, t) = 0$ i.e., the Chebyshev components obey $\sum_{k=0}^{N+2}(-1)^k p_k = 0$,
2. $u(-1, t) = 0$ i.e., $\sum_{k=0}^{N+2}(-1)^k u_k = 0$,
3. $\rho(1, t) = 0$ i.e., $\sum_{k=0}^{N+2} \rho_k = 0$.

2.3.1 Numerical Solution

The partial differential equation (9) can be expanded with the solution vector, P to form a system of partial differential equations as shown below.

$$\frac{\partial p}{\partial t} + \frac{\partial p}{\partial x} + \frac{\partial u}{\partial x} = 0, \qquad (10.a)$$

$$\frac{\partial u}{\partial t} + \frac{\partial p}{\partial x} + \frac{\partial u}{\partial x} = 0, \qquad (10.b)$$

$$\frac{\partial \rho}{\partial t} + \frac{\partial u}{\partial x} + \frac{\partial \rho}{\partial x} = 0. \qquad (10.c)$$

Expanding equation (10) using Chebyshev expansion by writing u as a finite series of Chebyshev polynomials as shown in equation (2), we get

$$\frac{\partial}{\partial t}\left[\sum_{k=0}^{N+2} p_k(t)T_k\,(x)\right]+\frac{\partial}{\partial x}\left[\sum_{k=0}^{N+2} p_k(t)T_k\,(x)\right]+\frac{\partial}{\partial x}\left[\sum_{k=0}^{N+2} u_k(t)T_k\,(x)\right]=0.$$

On differentiating we introduce the D matrix as discussed in the previous problem and the equation becomes

$$\sum_{k=0}^{N+2} \dot{p_k}(t)T_k(x)+\sum_{k=0}^{N+2} p_k\,(t)\sum_{r=0}^{N+2} D_{rk}T_r\,(x)+\sum_{k=0}^{N+2} u_k\,(t)\sum_{r=0}^{N+2} D_{rk}T_r\,(x)=0. \tag{11}$$

Applying the orthogonality principle, the above equation can be written as follows:

$$\int_{-1}^{1}\frac{[\sum_{k=0}^{N+2}\dot{p_k}\,(t)T_k(x)+\sum_{k=0}^{N+2}\sum_{r=0}^{N+2}p_k\,(t)D_{rk}T_r(x)+\sum_{k=0}^{N+2}\sum_{r=0}^{N+2}u_k\,(t)D_{rk}T_r(x)]T_i(x)}{\sqrt{(1-x^2)}}dx=0.$$

By applying these properties in the above equation, and after suitable algebra it reduces to

$$\dot{p}_\iota(t)+\sum_{k=0}^{N+2} D_{\iota k}p_k\,(t)+\sum_{k=0}^{N+2} D_{ik}u_k\,(t)=0, \tag{12}$$

Similarly equations (10.b) and (10.c) are solved using the orthogonal properties and the following equations are obtained.

$$\dot{u}_\iota(t)+\sum_{k=0}^{N+2} D_{\iota k}p_k\,(t)+\sum_{k=0}^{N+2} D_{ik}u_k\,(t)=0, \tag{13}$$

$$\dot{\rho}_\iota(t)+\sum_{k=0}^{N+2} D_{\iota k}u_k\,(t)+\sum_{k=0}^{N+2} D_{ik}\rho_k\,(t)=0. \tag{14}$$

Equations (12-14) are a set of ordinary differential equations that is tedious to solve analytically. These equations were solved successfully using the symbolic manipulator in MATLAB which can be understood by these relations below.

Let us consider matrix P to be

$$P_i = \left[p_{1,}\, p_{2,}\, \dots p_{N+2,} u_{1,}\, u_{2,}\, \dots u_{N+2,} \rho_{1,}\, \rho_{2,}\, \dots \rho_{N+2}\right],$$

which is of the order $[3(N+2),1]$.

Equation (12) can be written as

$$[I, O, O][\dot{P}] + [D, D, O][P] = 0 \tag{15}$$

where *O* is a matrix of size $[N+1, N+2]$ with all zeros, I is the identity matrix of size $[N+1, N+2]$ with all one's, *D* is a matrix of size $[N+1, N+2]$ with elements D_{ik} as discussed in section (2.1) and $\dot{P}$ is the solution vector.

Similarly equations (13) and (14) can be written as

$$[O, I, O][\dot{P}] + [D, D, O][P] = 0 \tag{16}$$

$$[O, O, I][\dot{P}] + [O, D, D][P] = 0 \tag{17}$$

Now, we write equations (15-17) in matrix form

$$M_1 \dot{P} + M_2 P = 0 \tag{18}$$

where, $M_1 = \begin{bmatrix} I & O & O \\ O & I & O \\ O & O & I \end{bmatrix}$ and $M_2 = \begin{bmatrix} D_1 & D_1 & O \\ D_1 & D_1 & O \\ O & O & D_1 \end{bmatrix}$

The boundary conditions are added and the range on integration is taken from 0 to 0.5. The tolerance is set to 10^{-9}. The initial conditions here are three as the number of dependent variables are three. The solver used is ODE45. The procedure is similar to that of the previous problem.

2.3.2 Exact Solution

The exact solution for the above problem is of the form

$$P_i = \sin((x+1)\pi - 2\,\pi t).$$

where, $x\,\epsilon\,(\pi, 2\pi)$ with *N* number of polynomials and t is the time step. The initial conditions are $P_i(x,0) = \sin[(x+1)\pi]$.

Figure 2.4 shows a comparison between the numerical and the exact solutions. The numerical results obtained are found to be in good agreement with the exact solution.

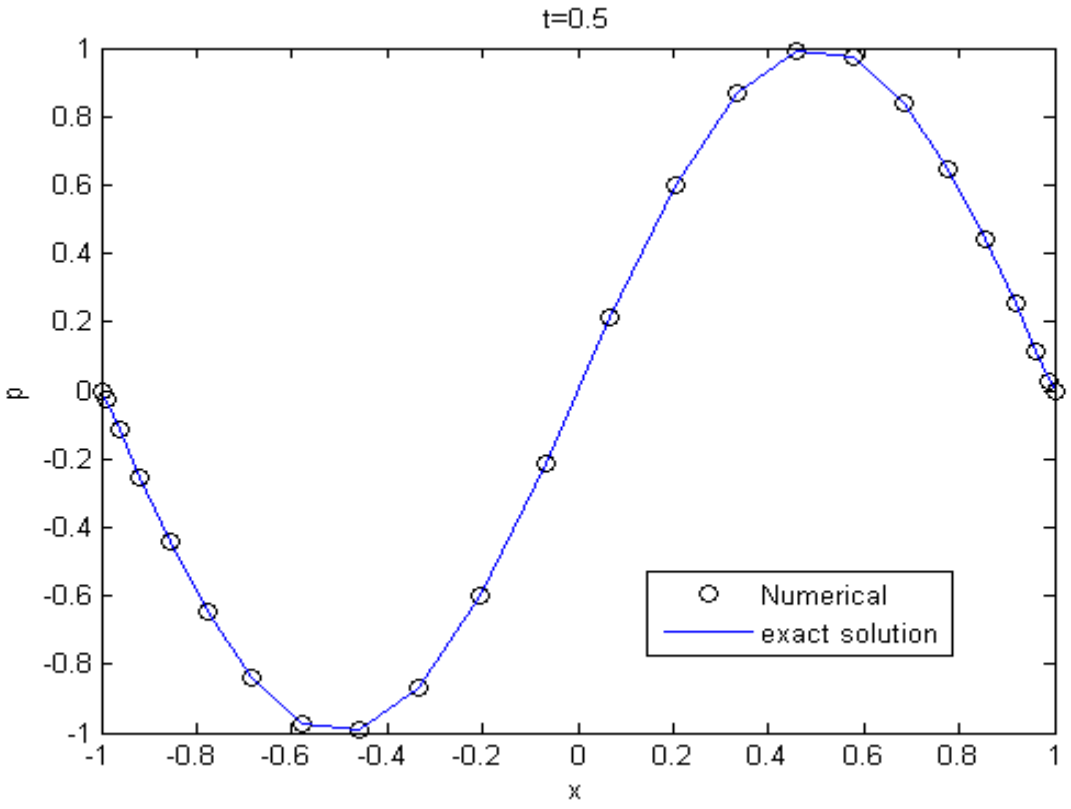

Figure 2.4: The sine curve showing the comparison between the numerical solution, denoted by O and exact solution, denoted by a solid line when $t = 0.5$.

2.3.3 Error

The error between the numerical solution and the exact solution is calculated by using the relation:

E_i (Error)= Numerical Chebyshev solution- Exact solution.

The graph obtained shows the error to be negligible and of the order 10^{-4}.

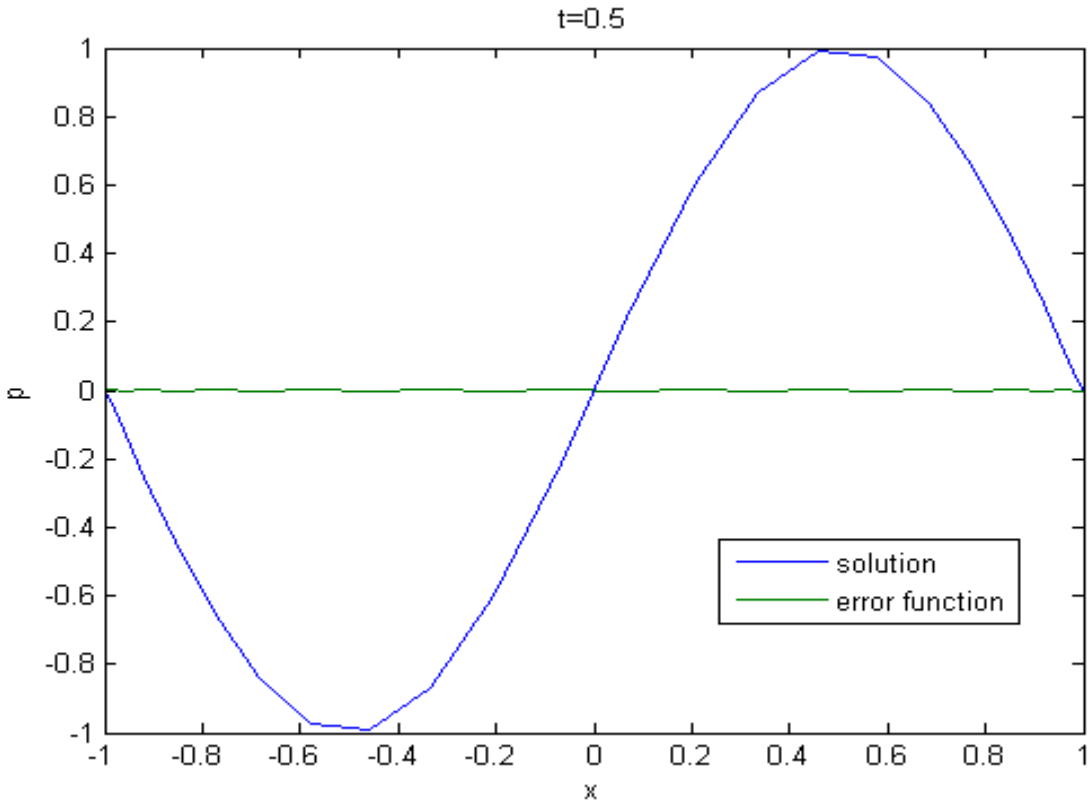

Figure 2.5: A graph showing the Chebyshev solution and the error (E_i) when $t = 0.5$.

2.3.4 Calculation of Error Root Mean Square

The root mean square (rms) of the error is calculated for a set of collocation points by using the relation,

$$rms=\sqrt{[\sum E_i^2]}/N.$$

The rms is calculated for $N = 4, 8, 12,$ and 24 is calculated by using the above relation and is given by,

rms= [1.1331, 0.0014, 2.2816e-005, 3.5452e-005]

Figure 2.6 shows the validation of the error rms against the number of Chebyshev polynomials N.

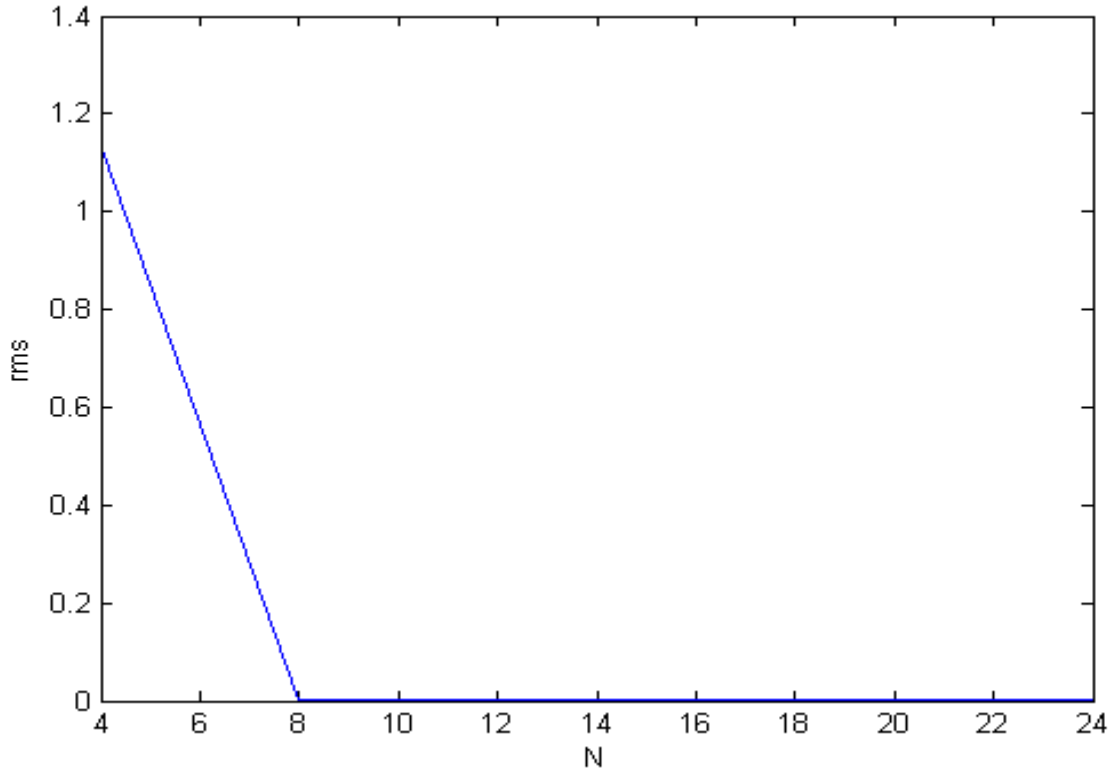

Figure 2.6: A graph showing the convergence of the solution at different N values.

2.4 Nonlinear 1-D Burger's Equation

Nonlinear partial differential equations occur in many fields of science and engineering with various applications in physics, chemistry and mathematics. The one-dimensional Burgers equation is important in understanding simplified model for turbulence, boundary layer behavior and mainly the formation of shocks.

In the following section the solution to the one-dimensional second-order nonlinear partial differential using Chebyshev-Tau method is discussed. The results obtained show a good agreement with the exact solution.

The 1D Burgers equation is of the form

$$\frac{\partial u}{\partial t} + \alpha u \frac{\partial u}{\partial x} - \nu \frac{\partial^2 u}{\partial x^2} = 0. \tag{19}$$

where, u is the velocity term, v is the viscosity, and α is an arbitrary constant.

2.4.1 Numerical Solution

Equation (19) is expanded using Chebyshev expansion by writing u as a finite series of Chebyshev polynomials.

$$u = \sum_{k=0}^{N+2} u_k \, T_k(x)$$

where N is the order of the maximum Chebyshev polynomial resolved in the truncation error, $T_k(x)$ is the Chebyshev polynomial of k_{th} order and u_k is the array of Chebyshev components. The expansion takes the form:

$$\frac{\partial}{\partial t}\left[\sum_{k=0}^{N+2} u_k T_k\,(x)\right] + \alpha \sum_{k=0}^{N+2} u_k T_k(x) \frac{\partial}{\partial x}\left[\sum_{r=0}^{N+2} u_r T_r\,(x)\right] - \nu \frac{\partial^2}{\partial x^2}\left[\sum_{k=0}^{N+2} u_k T_k\,(x)\right] = 0 \tag{20}$$

The first derivative (u_k^1) and second derivative (u_r^2) of u can be shown by the following expansions which are discussed in the work of Dongarra [9].

$$u_k^1 = \sum_{r=0}^{N+2} D_{kr} u_r$$

$$u_k^2 = \sum_{r=0}^{N+2} \sum_{s=0}^{N+2} D_{rk} D_{rs} \, u_r$$

Applying the orthogonality principle, the above equation (20) can be written as

$$\int_{-1}^{1} \frac{\left[\frac{\partial}{\partial t}\left[\sum_{k=0}^{N+2} u_k T_k\,(x)\right] + \alpha \sum_{k=0}^{N+2} u_k T_k(x) \frac{\partial}{\partial x}\left[\sum_{r=0}^{N+2} u_r T_r\,(x)\right] - \nu \frac{\partial^2}{\partial x^2}\left[\sum_{k=0}^{N+2} u_k T_k\,(x)\right]\right] T_i(x)}{\sqrt{(1-x^2)}} dx = 0.$$

The difficulty in solving of non linear equations is related to the appearance of integrals containing a triple of Chebyshev polynomials. It is handled in the following way:

$$\int_{-1}^{1} \frac{T_k(x)T_r(x)T_i(x)}{\sqrt{(1-x^2)}} dx = \frac{\pi}{2},$$

when $i = j + k$ or $j = i + k$ or $k = i + j$

Otherwise,

$$\int_{-1}^{1} \frac{T_k(x)T_r(x)T_i(x)}{\sqrt{(1-x^2)}} dx = \frac{1}{2}\left(\frac{\mathrm{Sin}[(i-j-k)\pi]}{i-j-k} + \frac{\mathrm{Sin}[(i+j-k)\pi]}{i+j-k} + \frac{\mathrm{Sin}[(i-j+k)\pi]}{i-j+k} + \frac{\mathrm{Sin}[(i+j+k)\pi]}{i+j+k}\right)$$

After some algebra the final form of equation is as shown below

$$\dot{u}_t + \alpha \sum_{k=0}^{N+2} D_{ik} u_k^2\,(t) - \nu \sum_{k=0}^{N+2} D_{ik}^2 u_k\,(t) = 0. \qquad (21)$$

2.4.2 Exact Solution

Consider the Burgers Equation:

$$\frac{\partial u}{\partial t} + \alpha u \frac{\partial u}{\partial x} - \nu \frac{\partial^2 u}{\partial x^2} = 0,\ x \in Dx[0, T],$$

with the wave solutions

$$u(x,t) = \frac{c}{\alpha} + \left(\frac{2\nu}{\alpha}\right) \tanh(x - ct),$$

where, $c = 0.1,\ \nu = -0.0001$ and $\alpha = 1$. The solution domain is $D = \{x: a < x < b\}$; with α and ν as arbitrary constants [10].

Figure 2.7 shows a comparison between the solution obtained numerically using Chebyshev polynomials which is marked as O and the exact solution which is marked with a solid line. The numerical results obtained are found to be in good agreement with the exact solution.

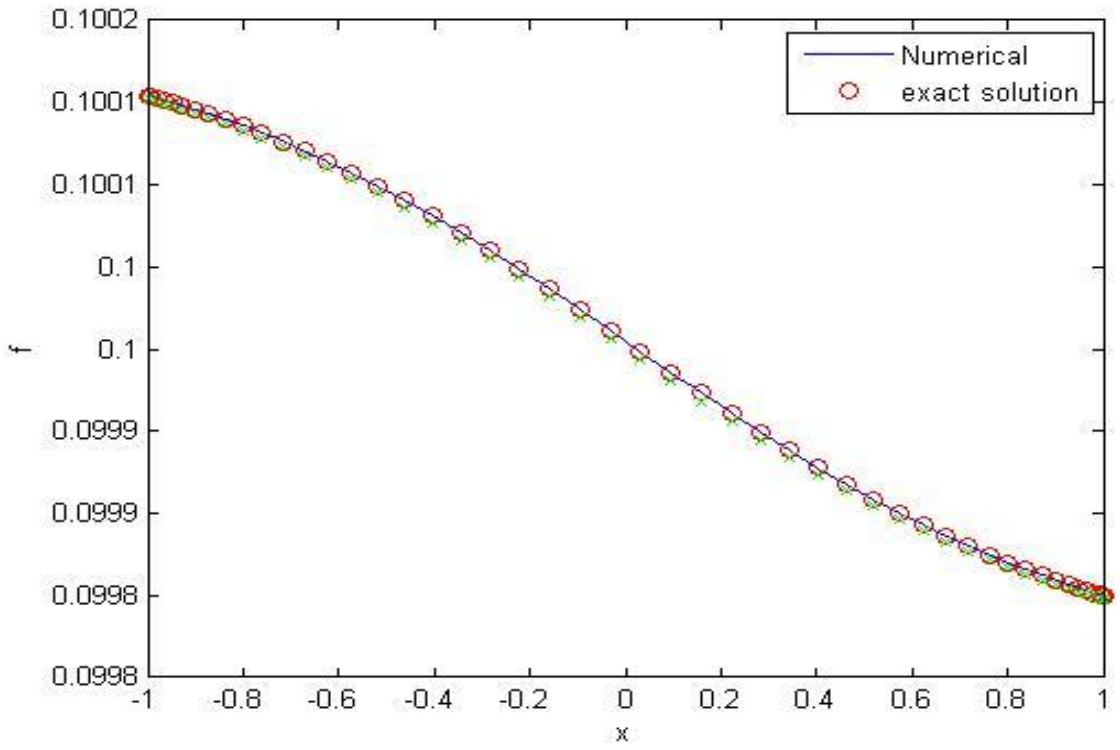

Figure 2.7: A graph showing the numerical solution denoted by a solid line and the exact solution denoted by O.

2.4.3 Error

Figure 2.8 shows the error which is the difference between the numerical solution and the exact solution at each location for the number of Chebyshev polynomials, $N = 10$ and $N = 20$.

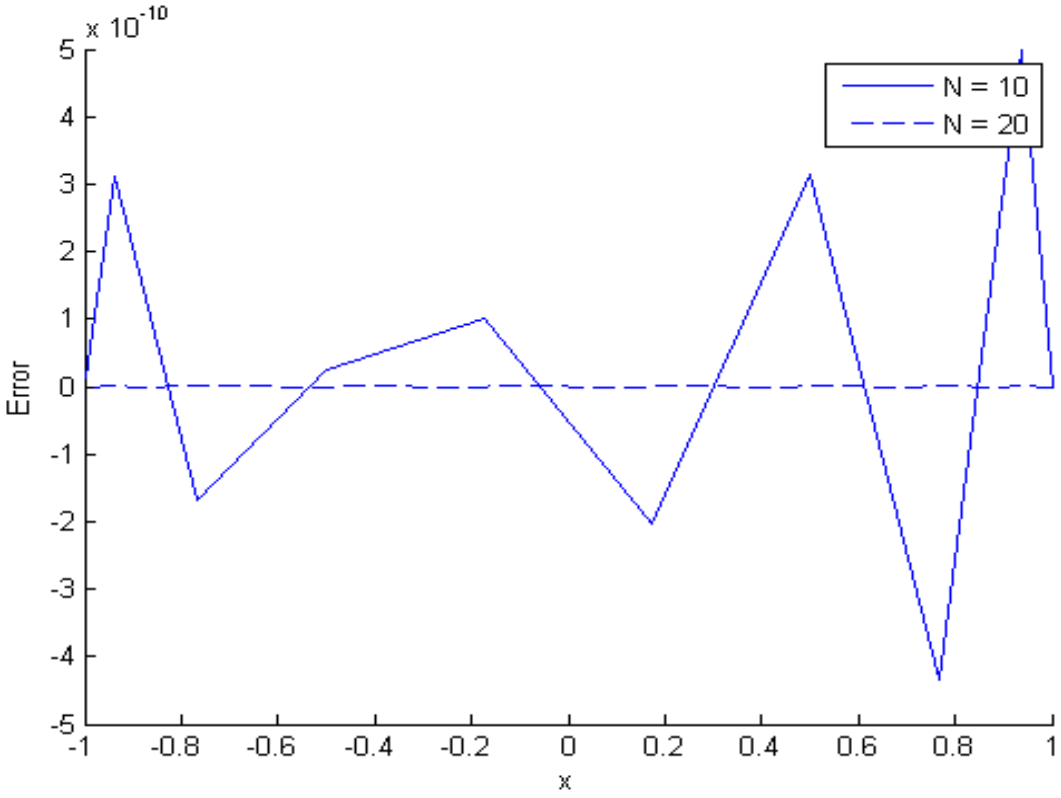

Figure 2.8: A plot showing the Error for $N = 10$ and $N = 20$

CHAPTER 3

THE REACTIVE RMI PROBLEM

3.1 Introduction

The objective of this section is to identify the dynamics of a perturbation of a planar interface between two fluids of different density when subject to instantaneous shock acceleration. We shall do so by assuming that the perturbation is much smaller than the base flow, and thus by linearizing the dynamic equations. The focus of the research is on the effect of the reactivity of the mixture on perturbation growth.

3.2 Initialization of the Problem

Consider a planar shock incident on an interface that separates two fluids of different density Figure 3.1. The two dimensional plane has Cartesian coordinates *x* and *y*, to which correspond unitary vectors $\vec{\imath}$ and $\vec{\jmath}$. At time $t = t_0$ the shock impinges the interface, a reflected rarefaction (i.e., the expansion fan), and a transmitted corrugated shocks depart from the point of impact [8] as shown in Figure 3.2. There are three interfaces in the system, the expansion fan labeled as (r), the transmitted shock labeled as (t), and the contact interface labeled as (I). The interfaces move with time/space dependent velocities, $W_r(t,y)$, $W_t(t,y)$ and $W_I(t,y)$ with the directions as indicated in Figure 3.2. The reflected expansion-transmitted shock system divides the space in 4 regions labeled in Figure 3.2 as region (0) to the left of the transmitted shock, region (1), region (2) and region (3) to the right of the transmitted shock.

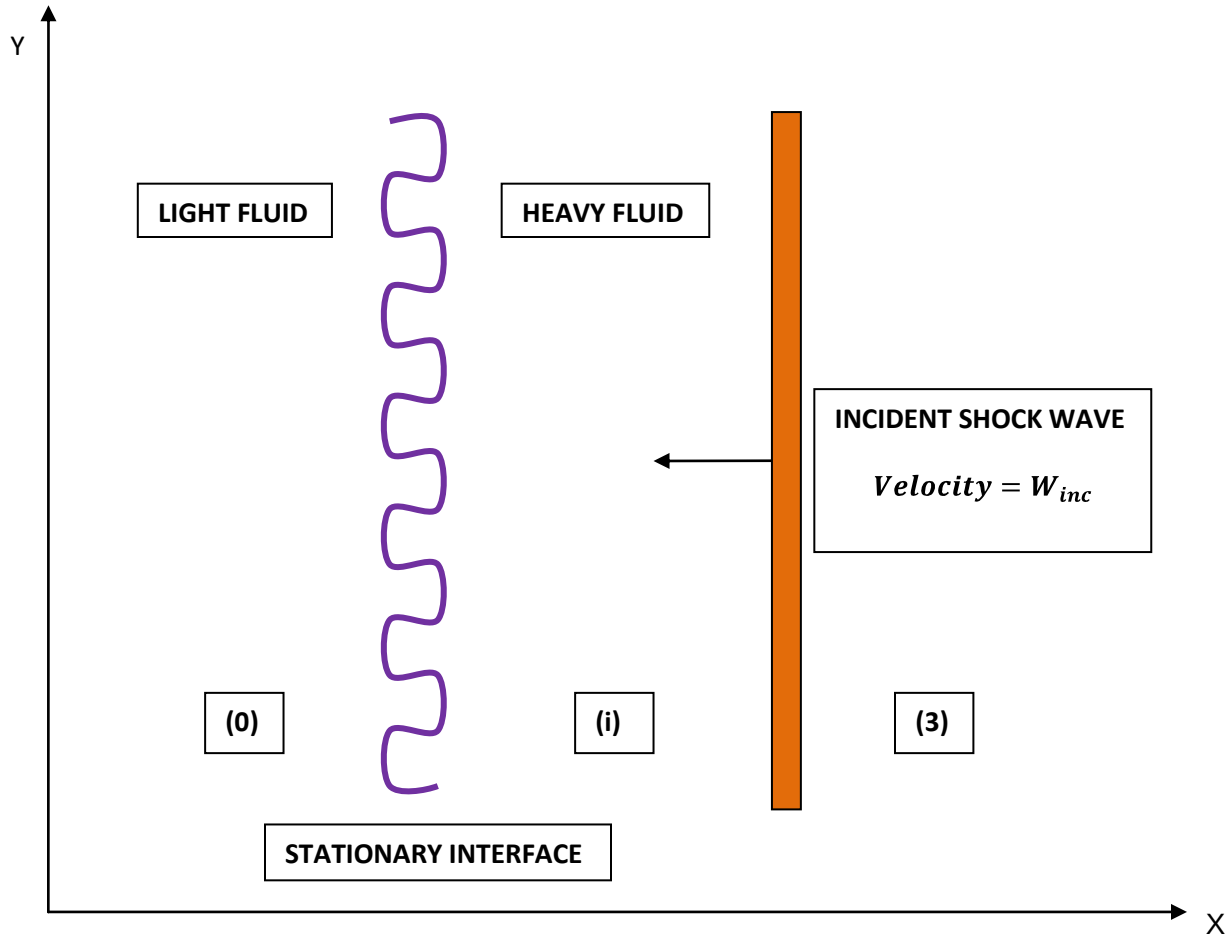

Figure 3.1: Incident shock wave

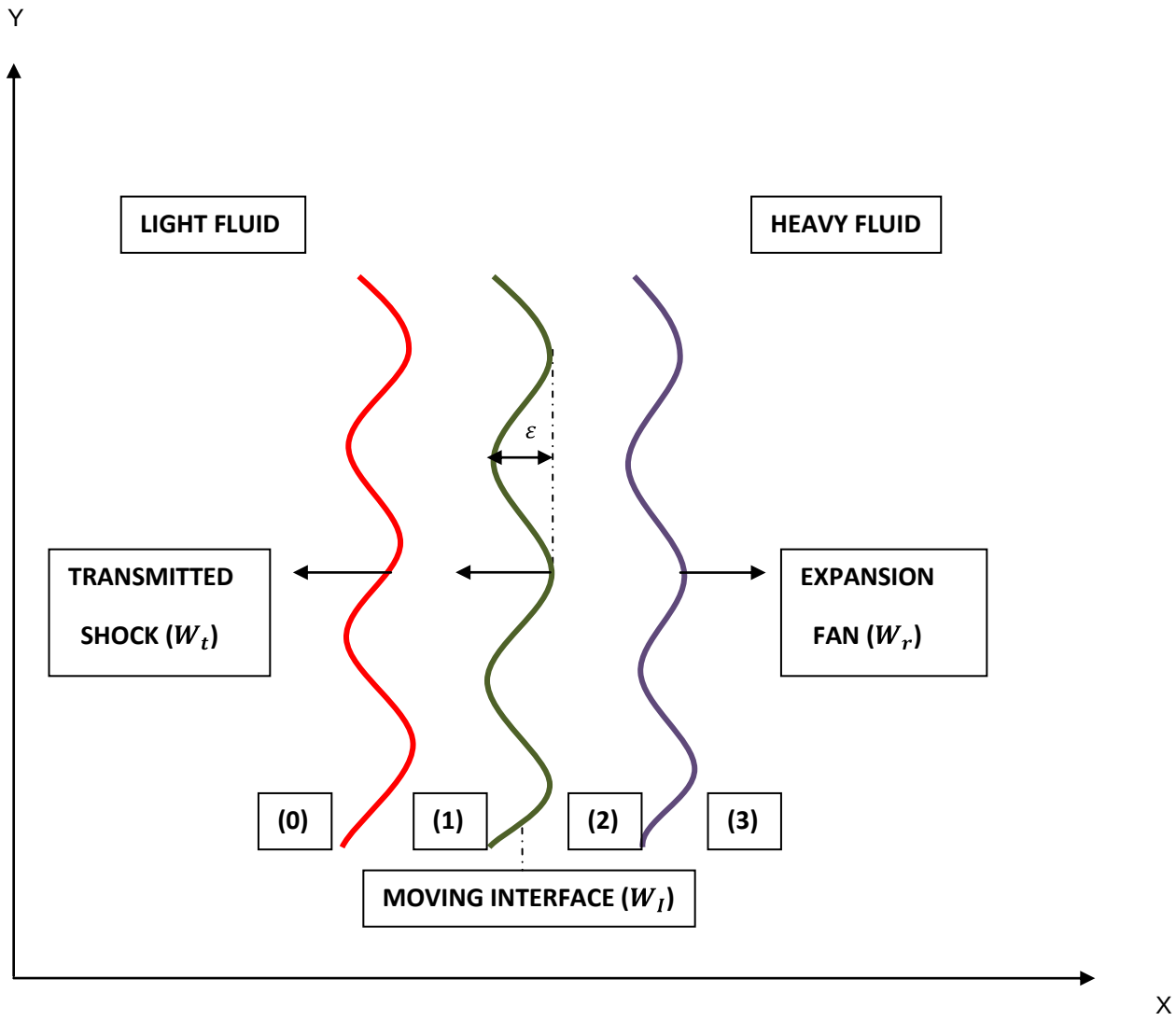

Figure 3.2: Expansion fan and transmitted shock formed with the incident shock wave.

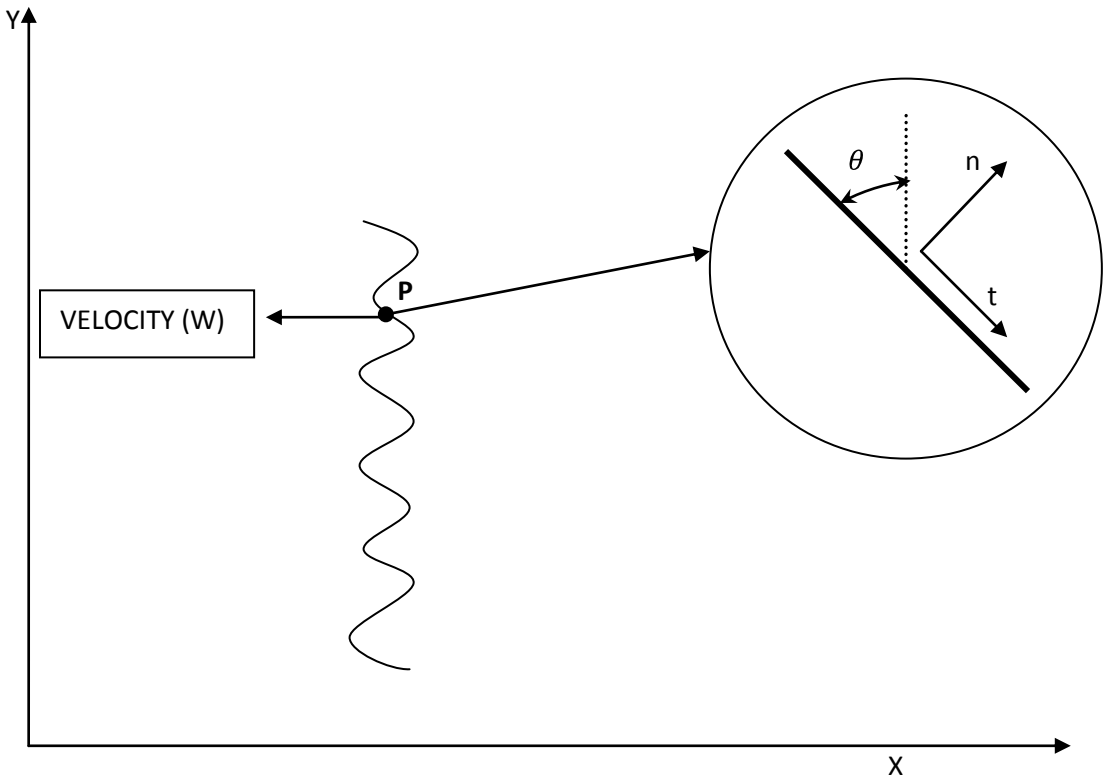

Figure 3.3: Local conditions at any interface (shocks, or contact discontinuity).

We seek to evaluate the time dependent solution to the problem, *i.e.*, the pressure p, velocity vector $\vec{u} \equiv u\vec{\imath} + v\vec{\jmath}$, the density ρ, and reaction progress variable λ. The solution vector is written as

$$P(x, y, t) = [p, u, v, \rho, \lambda]^T. \tag{22}$$

The solution vector is expanded in the sum of a base solution (zeroth-order solution) and a perturbation (first-order solution):

$$P(x, y, t) = P^0(x, y) + P^1(x, y, t)\, \varepsilon \sin ky\ . \tag{23}$$

Note that if there were no combustion, the zeroth-order solution would not be a function of the spatial coordinates or the time.

3.3 Governing Equations

The governing equations are the Euler equations for a reactive flow. The region of the space of the incident shock i.e., regions (3) and (i) as shown in Figure 3.2 are connected using the Rankine-Hugoniot conditions. Also, regions (0) and (1) shown in Figure 3.2 are connected with the Rankine-Hugoniot relations. The Rankine-Hugoniot equations are written in terms of local conditions at the interface. First, for each point (P) on the interface, we define a local reference system (t, n) moving at the interface speed and aligned with it, as shown in Figure 3.3.

$$u_n = (u - W)\cos\theta + v\,sin\,\theta\,, \tag{24.a}$$

$$u_t = -u\sin\theta + v\cos\theta\,. \tag{24.b}$$

Next, for each interface we define a jump operator $[.]$ that yields the difference between the quantity at the right of the interface (R) and the quantities at the left of it (L). Additionally, we introduce the assumption of thermally and calorically perfect gases with isentropic index γ, and introduce the total enthalpy

$$H = \frac{\gamma}{\gamma - 1}\frac{p}{\rho} - Q\lambda + \frac{1}{2}(u_n^2 + u_t^2),$$

We shall also consider the incident shock, labeled as (inc), when solving for the flow. These equations are as shown below. Note that $\lambda = 0$ since there is no reaction in the zeroth-order solution.

The Rankine-Hugoniot relations are written as:

$$[\,\rho u_n] = 0, \tag{25.a}$$

$$[p + \rho u_n^2] = 0, \tag{25.b}$$

$$[H] = 0, \tag{25.c}$$

$$[u_t] = 0, \qquad (25.d)$$

$$[\lambda] = 0. \qquad (25.\mathrm{e})$$

3.4 Conditions to Initiate the Shock

The thermodynamic quantities across the incident shockwave are related by the Rankine-Hugoniot relations. For the regions between (i) and (3) in the figure 3.1 the Hugoniot relations allow us to calculate the initial conditions by solving a shock-contact Riemann solver. Based on the geometry and scales, we get $u_i = 0, \rho_0 = 1, P_0 = 1, \frac{m_i}{m_0} = 2, \ \rho_i = \rho_0 * \frac{m_i}{m_0}$.

At the incident shock

$$\rho_i u_{ni} + \rho_3 u_{n3i} = 0,$$

$$P_i + \rho_i {u_{ni}}^2 - P_3 + \rho_3 {u_{n3i}}^2 = 0,$$

$$H_i - H_{3i} = 0\,.$$

where,

$$u_{ni} = u_i - w_i\,,$$

$$u_{n3i} = u_3 - w_i\,,$$

$$H_i = \frac{\gamma}{\gamma-1}\frac{p_i}{\rho_i} + \frac{1}{2}({u_{ni}}^2),$$

$$H_{3i} = \frac{\gamma}{\gamma-1}\frac{p_3}{\rho_3} + \frac{1}{2}({u_{n3i}}^2),$$

w_i is the velocity of the shock, u_i is the velocity of the wave in the region *i* , towards the left of the incident shock, and u_3 velocity of the wave in the region 3 towards the right of incident the shock. Also, p_i , ρ_i, p_3, ρ_3 are the pressures and densities in regions *i* and 3 respectively.

By solving the above equations we can find the initial conditions to initiate the shock i.e.,u_3, ρ_3 w_i, and Mach number M_I are given as follows:

$$u_3 = \frac{\sqrt{2}(-1+p_3)}{\sqrt{\frac{m_i}{m_0}(-1+\gamma+p_3+\gamma p_3)}},$$

$$\rho_3 = \frac{\frac{m_i}{m_0}(-1+\gamma+\mathrm{p3}+\gamma p_3)}{1+\gamma+(-1+\gamma)p_3},$$

$$w_i = \frac{\sqrt{-1+\gamma+p_3+\gamma p_3}}{\sqrt{2}\sqrt{\frac{m_i}{m_0}}},$$

$$M_I = \frac{w_i}{\sqrt{(\frac{\gamma p_0}{\rho_i})}}.$$

3.5 Scales and Parameters

The pressure, density and the temperature are the variables in region (0) of figure 3.2. The velocity scale is obtained by taking the square root of the ratio between the reference pressure and density, $i.e.,$ $u_0 = \sqrt{\frac{p_0}{\rho_0}}$.

The length scale is the inverse of the wave number k. The time scale is based on the reference length and velocity. $i.e.,$ $T = \frac{L}{u_0}$, where, $L = \frac{1}{k}$.

The transition of a shock from non reactive to a reactive mixture is considered in the present work. The Figure 3.2 shows two regions, region (1) and region (2). The reactive mixture is in region (1) and the

non-reactive mixture is in region (2). Assuming that there is steady detonation in region (1) the non-dimensional parameters are needed to find the solution. The first three non-dimensional parameters considered to obtain the solution of non-dimensional problem are activation energy E, heat release Q, isentropic index γ. The isentropic index γ is set to be 1.2 in this entire research. If the half reaction distance is taken as the length scale, the perturbation is given by the product of the half reaction distance $L_{1/2}$ and the wave number$k$.

The selection of wave number as length scale is due to the fact that the Richtmyer-Meshkov instability is dominant over the detonation intrinsic instability, and the transversal wave length is the only scale on non-reactive problem. The fourth parameter is the density ratio across the stationary interface and the region (1) shown in the Figure 3.2. The density ratio in this problem is represented as $\frac{m_i}{m_0}$ and is equal to 2.

These four non-dimensional parameters lead to the determination of all other non-dimensional variables that describe the system. These parameters are varied to study their effect on the instability. The isentropic index and the density ratio are kept constant. The value of heat release and activation energy will be changed at the same rate to simulate the effect of changing the un-reacted stream temperature.

CHAPTER 4

SOLVING THE SHOCK SYSTEM

4.1 Transmitted Shock Wave

Equations (26) are also valid at the interface separating the regions (0) and (1). Solving these equations we can find the unknowns u_1, ρ_1, w_1 and the Mach number M_1 which describe the flow variables of the transmitted shock wave. The following are the flow properties obtained by solving the jump conditions at the interface of the transmitted shock wave.

$$u_1 = \sqrt{2}\sqrt{\frac{(-1+p_1)^2}{-1+\gamma+p_1+\gamma p_1}},$$

$$\rho_1 = \frac{-1+\gamma+p_1+\gamma p_1}{1+\gamma+(-1+\gamma)p_1},$$

$$w_1 = \frac{-1+p_1}{\sqrt{2}\sqrt{\frac{(-1+p_1)^2}{-1+\gamma+p_1+\gamma p_1}}},$$

$$M_1 = \frac{w_1}{\sqrt{\gamma\frac{p_0}{\rho_0}}}.$$

4.2 Expansion Fan Region

The fundamental difference between the Riemann problem under investigation and that supporting the classical RMI is the absence of a reflected shock. The transition of the shock from the heavy to light mixture induces an expansion fan, the solution of which is described in this section. The base flow is one-dimensional and reactive. Regions (2) and (3) as shown in the Figure 3.2 represent the post shock invariant flame conditions.

From the concept of method of characteristics, it is evident that the C^- , left running characteristic at the interface is equal to the C^- characteristic at region (3) in the Figure 3.2. The Riemann invariant J^- at the interface and at region (3) are as shown below.

Hence the J^- at the interface is defined as

$$J_I^- = u_1 - \frac{2\sqrt{\gamma(\frac{p_1}{\rho_2})}}{(\gamma-1)},$$

where,

$$\rho_2 = (\frac{p_2}{p_3})^{\frac{1}{\gamma}}\rho_3.$$

At the interface, $p_1 = p_2$ and $u_1 = u_2 = w_I$

J^- at the region (3) is defined as,

$$J_3^- = u_3 - \frac{2\sqrt{\gamma(\frac{p_3}{\rho_3})}}{(\gamma-1)},$$

$J_I^- = J_3^-$.By equating J_I^- and J_3^- we solve for P_1 which is the pressure at region (1) in the Figure 3.2.

4.3 The Reactive Euler Equations

The reactive Euler equations control the time evolution of the solution in region (1) as shown Figure 3.2. We start with the conservative variable formulation,

$$\frac{\partial K}{\partial t}+\frac{\partial F}{\partial x}+\frac{\partial G}{\partial y}+R_1=0. \tag{26}$$

where,

$$K=\begin{bmatrix}\rho\\ \rho u\\ \rho v\\ \rho[\frac{1}{\gamma-1}\frac{p}{\rho}-Q\lambda+\frac{1}{2}(u^2+v^2)\\ \rho\lambda\end{bmatrix} \tag{27.a}$$

$$F=\begin{bmatrix}\rho u\\ p+\rho u^2\\ \rho uv\\ \rho uH\\ \rho u\lambda\end{bmatrix} \tag{27.b}$$

$$G=\begin{bmatrix}\rho v\\ puv\\ p+\rho v^2\\ \rho vH\\ \rho v\lambda\end{bmatrix} \tag{27.c}$$

$$R_1=\begin{bmatrix}0\\ 0\\ 0\\ 0\\ -\rho\dot{\omega}\end{bmatrix} \tag{27.d}$$

and $\dot{\omega} \equiv (1-\lambda)A_{\omega}exp^{-E_{\omega}\frac{\rho}{p}}$ is the rate of destruction of mass of reactant per unit mass of mixture. It is useful to transform the Euler equations in primitive variables, *P.* (See equation (22)). To do so we evaluate a set of Jacobian matrices, $Q_P \equiv \frac{\partial \mathrm{K}}{\partial \mathrm{P}}$, $A_1 \equiv \frac{\partial \mathrm{F}}{\partial \mathrm{P}}$ and $B_1 \equiv \frac{\partial \mathrm{G}}{\partial \mathrm{P}}$, write the Euler equations as

$$\frac{\partial P}{\partial t} + Q_P^{-1}A_1\frac{\partial P}{\partial x} + Q_P^{-1}B_1\frac{\partial P}{\partial y} + Q_P^{-1}R_1 = 0 \qquad (28)$$

We denote,

$$A \equiv Q_P^{-1}A_1,\ B \equiv Q_P^{-1}B_1 \text{ and } R \equiv Q_P^{-1}R_1$$

Equation (28) is now written as shown below

$$\frac{\partial P}{\partial t} + A\frac{\partial P}{\partial x} + B\frac{\partial P}{\partial y} + R = 0 \qquad (29)$$

We calculate the Jacobian matrices and obtain the A, B and R matrices.

$$A = \begin{bmatrix} u & \gamma p & 0 & 0 & 0 \\ \frac{1}{\rho} & u & 0 & 0 & 0 \\ 0 & 0 & u & 0 & 0 \\ 0 & \rho & 0 & u & 0 \\ 0 & 0 & 0 & 0 & u \end{bmatrix}$$

$$B = \begin{bmatrix} v & 0 & \gamma p & 0 & 0 \\ 0 & v & 0 & 0 & 0 \\ \frac{1}{\rho} & 0 & v & 0 & 0 \\ 0 & 0 & \rho & v & 0 \\ 0 & 0 & 0 & 0 & v \end{bmatrix}$$

$$R = \begin{bmatrix} 0 \\ 0 \\ 0 \\ -\rho\,\dot{\omega} \end{bmatrix}.$$

We also define the first variation of the matrix *A* that will be used in the perturbation expansion of the Euler equations:

$$A^1 = \begin{bmatrix} -\frac{E(-1+\gamma)Q\,\rho^2\dot{\omega}}{p^2} & 0 & 0 & -\frac{(-1+\gamma)Q(p-E\,\rho)\dot{\omega}}{p} & -(-1+\gamma)Q\rho\frac{\partial\dot{\omega}}{\partial\lambda} \\ 0 & 0 & 0 & 0 & 0 \\ 0 & 0 & 0 & 0 & 0 \\ 0 & 0 & 0 & 0 & 0 \\ -\frac{E\rho\dot{\omega}}{p^2} & 0 & 0 & \frac{E\dot{\omega}}{p} & -\frac{\partial\dot{\omega}}{\partial\lambda} \end{bmatrix}.$$

4.4 Coordinate Transformation

A coordinate transformation is necessary to map the time-dependent solution domain in a stationary one. We concentrate on region (1). We transform the domain between the two moving shocks into a stationary domain between two flat shocks. The mapping is illustrated in Figure 4.1.

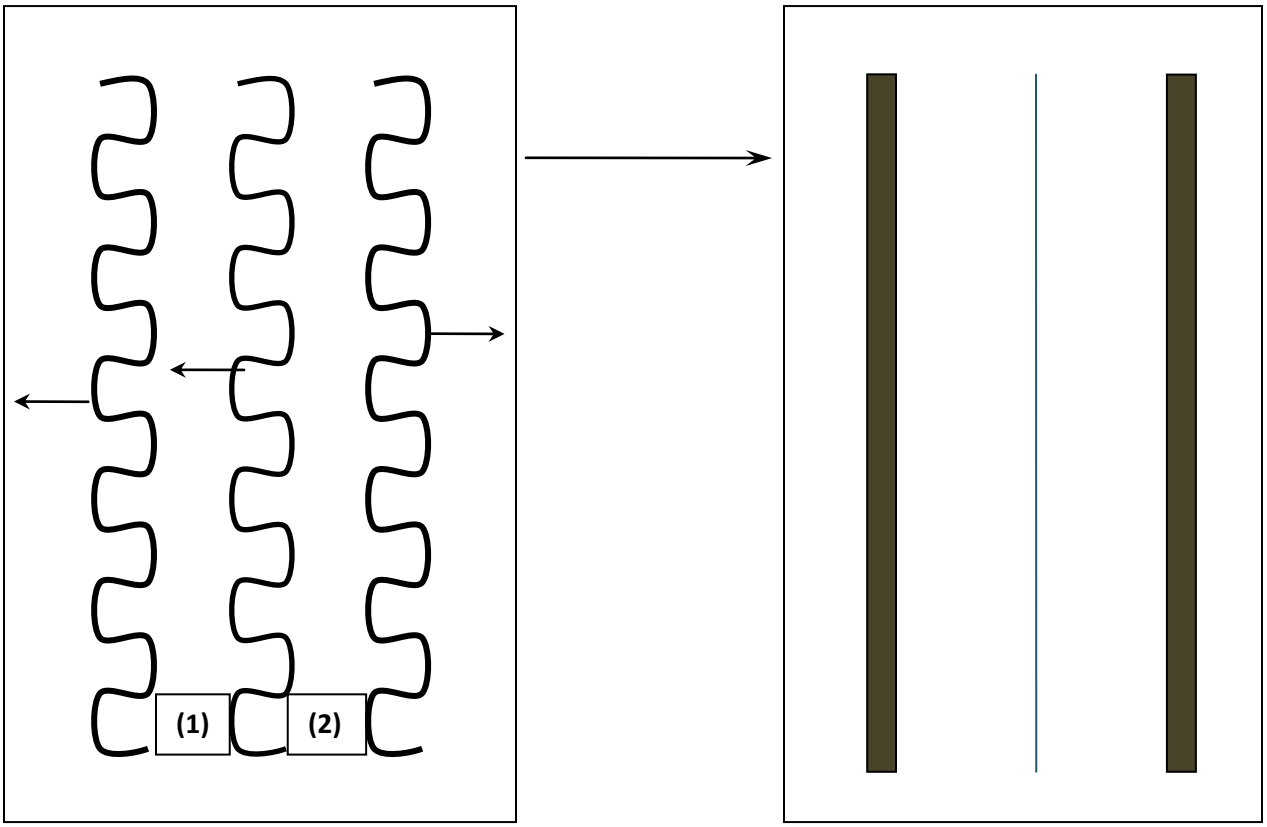

Figure 4.1: Schematic of mapping.

Consider region (1) and assume that the coordinate of the two interfaces that delimit it are given as $x_1(y,t)$ and $x_2(y,t)$ for the left and right interfaces, respectively. We define a new coordinate system (τ,ξ,η) related to by (t,x,y) by

$$x = x_1 + \frac{x_2 - x_1}{2}(\xi + 1)\,, \quad \xi \in (-1,1), \tag{30.a}$$

$$y = \eta, \quad \eta \in (-\infty,\infty), \tag{30.b}$$

$$t = \tau, \quad \tau \in (0,\infty), \tag{30.c}$$

For the sake of a short hand notation, we define three auxiliary variables,

$$\beta_1 = -\frac{\xi - 1}{2}, \quad \beta_2 = 1 - \beta_1 \text{ and } \delta = \sum_{j=1}^{2} \frac{\partial \beta_j}{\partial \xi} x_j \tag{31}$$

As customary in coordinate transformations, the next step is to determine derivatives with respect to (t, x and y) in terms of derivatives with respect to (τ, ξ, η) .

For any variable $\psi = (t, x, y)$, we find

$$\frac{\partial \psi}{\partial x} = \frac{\partial \psi}{\partial \xi} / \delta \tag{32.a}$$

$$\frac{\partial \psi}{\partial t} = \frac{\partial \psi}{\partial \tau} - \left(\sum_{j=1}^{2} \beta_j \frac{\partial x_j}{\partial t} \right) \frac{\partial \psi}{\partial \xi} / \delta \tag{32.b}$$

$$\frac{\partial \psi}{\partial y} = \frac{\partial \psi}{\partial \eta} - \left(\sum_{j=1}^{2} \beta_j \frac{\partial x_j}{\partial y} \right) \frac{\partial \psi}{\partial \xi} / \delta \tag{32.c}$$

4.5 Linearized Zeroth-Order Equation

Substitution of the mapping relations, equation (32), into the Euler equation, equation (29), yields a set of non-linear equations. Using equation equation (22) for the primitive variables, and collecting term of equal perturbation order yields two linear equations, one for the zeroth-order, P^0, and one for the first order perturbation, P^1. In the non-reactive case, the zeroth-order equation reduces to P^0 = constant over both regions (1) and (2) in Figure 3.2. For the reactive case, the equation is non-linear and is given by

$$\frac{\partial P^0}{\partial \tau} + \left(\frac{A^0}{\delta^0} - \sum_{J=1}^{2} \frac{\beta_j}{\delta^0} W_j^0 I \right) \frac{\partial P^0}{\partial \xi} + R(P^0) = 0 \tag{33}$$

4.6 First-Order Perturbation Equation

Before discussing the first-order equation, we adopt a nomenclature similar to Richtmyer's [1] equations (6-8), and set,

$$x_j = W_j^0 t + \overline{a}_j(t, y) \tag{34}$$

where, W_j^0 is the velocity of the shock. $\overline{a}_j(t, y)$ is given as

$$\overline{a}_j(t, y) = a_j(t)\varepsilon \sin ky$$

The time derivatives of the corrugation terms with respect to the time $\dot{a}_j$ will be identified as the deformation rates, *i.e.*, $\dot{a}_I$ is the interface deformation rate. Thus, we obtain the following expansions,

$$\delta^0 = \left(\sum_{J=1}^{2} \frac{d\beta_j}{d\xi} W_j^0 \right) t\,, \tag{35.a}$$

$$\delta^1 = \sum_{J=1}^{2} \frac{d\beta_j}{d\xi} a_j(t, y), \tag{35.b}$$

In the linearized analysis we assume (for both reactive and non-reactive fluids) the $y \equiv \eta$ direction to be homogeneous. Thus the zeroth-order solution does not depend on η. Derivatives of the first-order perturbation with respect to η are determined by multiplying the value of the function by the term ik, where i is the imaginary unit and k is the wave number of the perturbation, *i.e.*,

$$\frac{\partial \psi}{\partial \eta} = ik\psi$$

The first-order perturbation equation becomes after some manipulation,

$$\frac{\partial P^1}{\partial \tau}+\frac{\delta^{\,1}}{\delta^{\,0}}\left(\frac{\partial P^0}{\partial \tau}+R(P^0)\right)-\left(\sum_{J=1}^{2}\frac{\beta_j}{\delta^{\,0}}\dot{a_j}\right)\frac{\partial P^0}{\partial \xi}-ik\left(\sum_{J=1}^{2}\frac{\beta_j}{\delta^{\,0}}a_j\right)B^0\frac{\partial P^0}{\partial \xi}+\left(\frac{A^0}{\delta^{\,0}}-\sum_{J=1}^{2}\frac{\beta_j}{\delta^{\,0}}W_j^0 I\right)\frac{\partial P^1}{\partial \xi}$$

$$+ikB^0P^1+\frac{\partial R}{\partial P}P^1+\frac{A^1\frac{\partial P^0}{\partial \xi}}{\delta^{\,0}}=0 \qquad (36)$$

CHAPTER 5

BASE FLOW - THE ZEROTH-ORDER SOLUTION

5.1 Initial Conditions

The initial conditions are given at $t = 0,\ \delta_0 = 0$. The zeroth-order solution is taken piecewise constant in region (1). The shock and the contact discontinuity yield the values for the flow variables. The time derivatives at the initial time is evaluated by taking the limit for $t \to 0^+$ (i.e., just as the shock impinges the interface) of equation (33).

By using L' Hospital's rule the initial derivative $\dot{P}$ is found by solving

$$\frac{\partial \dot{P}}{\partial \tau} + \frac{A^0 - \sum_{j=1}^{2} \beta_j W_j^0 I}{(\sum_{j=1}^{2} \frac{d\beta_j}{d\xi} W_j^0)} \frac{\partial \dot{P}}{\partial \xi} + R(P^0) = 0 \qquad (37)$$

where, $P^0, W^0 \; and \; A^0$ are evaluated at initial time. Equation (37) along with the boundary conditions on $\dot{P}$ is obtained from differentiating the shock conditions, are solved using the same discretization as for the time dependent problem. Note:

$$\frac{\partial P^0}{\partial x} = \lim_{t \to 0^+} (\frac{\partial P^0}{\partial \xi} / \delta^0) \neq 0$$

leads to $\lim_{t \to 0^+} (\frac{\partial \dot{P}}{\partial \xi}) \neq 0$, as a consequence of the boundary conditions, which implies that

$$\lim_{t \to 0^+} (\frac{\partial P^0}{\partial \xi} + R(P^0)) \neq 0 \qquad (38)$$

5.2 The Zeroth-Order Solution in Transmitted Shock Region

By solving the zeroth-order equation (33) we obtain the time varying components of pressure, velocity, density and rate of reaction at each collocation points. These components are obtained by expanding the solution in Chebyshev polynomials. Figure 5.1 shows the pressure calculated at each collocation point in the transmitted shock region when $time = 87.9066$. It is observed that, the pressure tends to increase with the formation of detonation wave, eventually decreases and becomes constant.

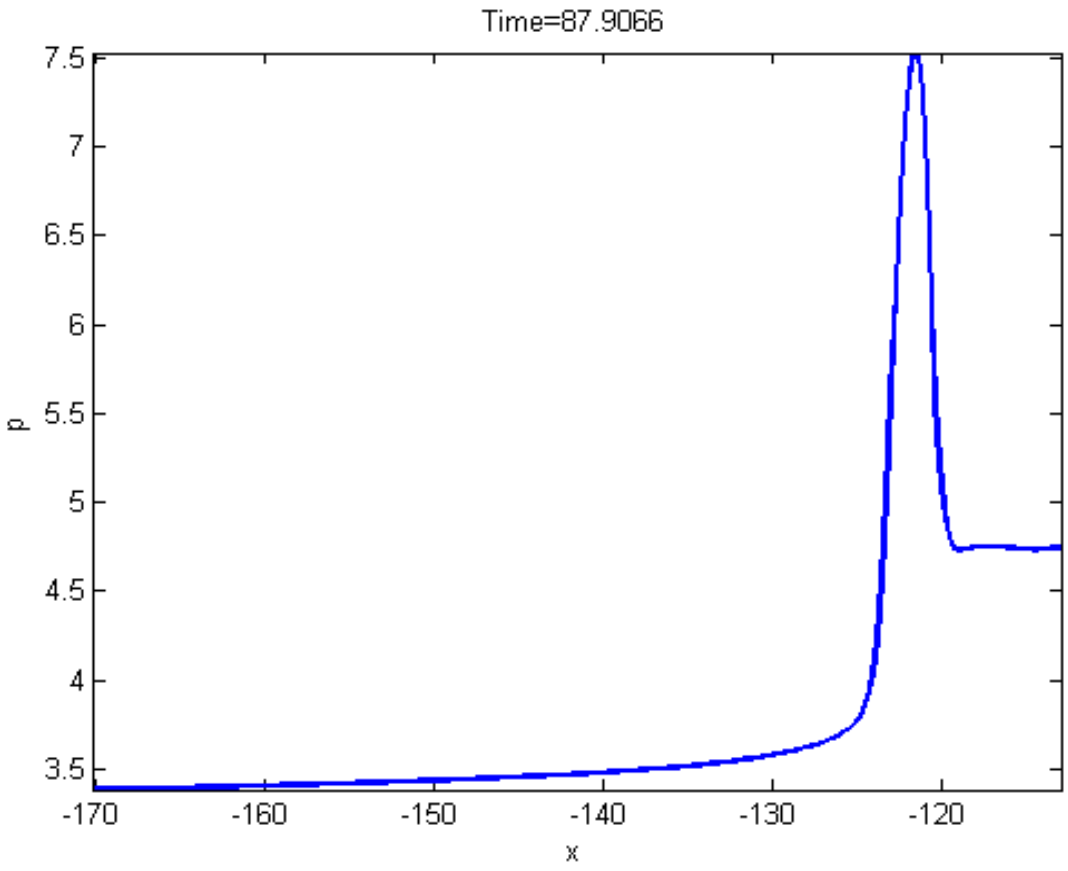

Figure 5.1: Pressure p obtained at different locations x in the transmitted shock region when $t = 87.9$.

Figure 5.2 shows the velocity components at each collocation point when $time = 87.9066$. The plot shows the decrease in the velocity of the transmitted shock wave in the region where the detonation wave is formed. The velocity increases gradually and becomes constant.

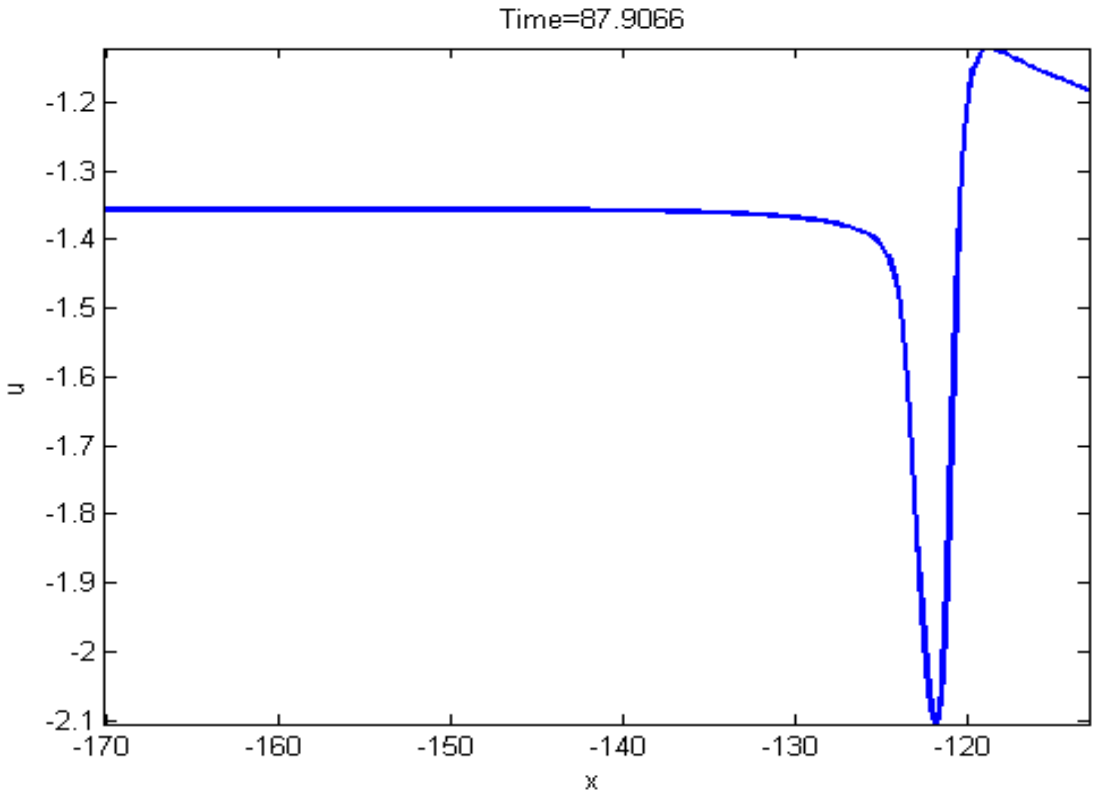

Figure 5.2: Velocity u obtained at different locations x in the transmitted shock region when $t = 87.9$.

Figure 5.3 shows the density obtained at different points when $time = 87.9066$. The figure explains that there is a sharp increase in density when the detonation wave is formed and it further becomes constant.

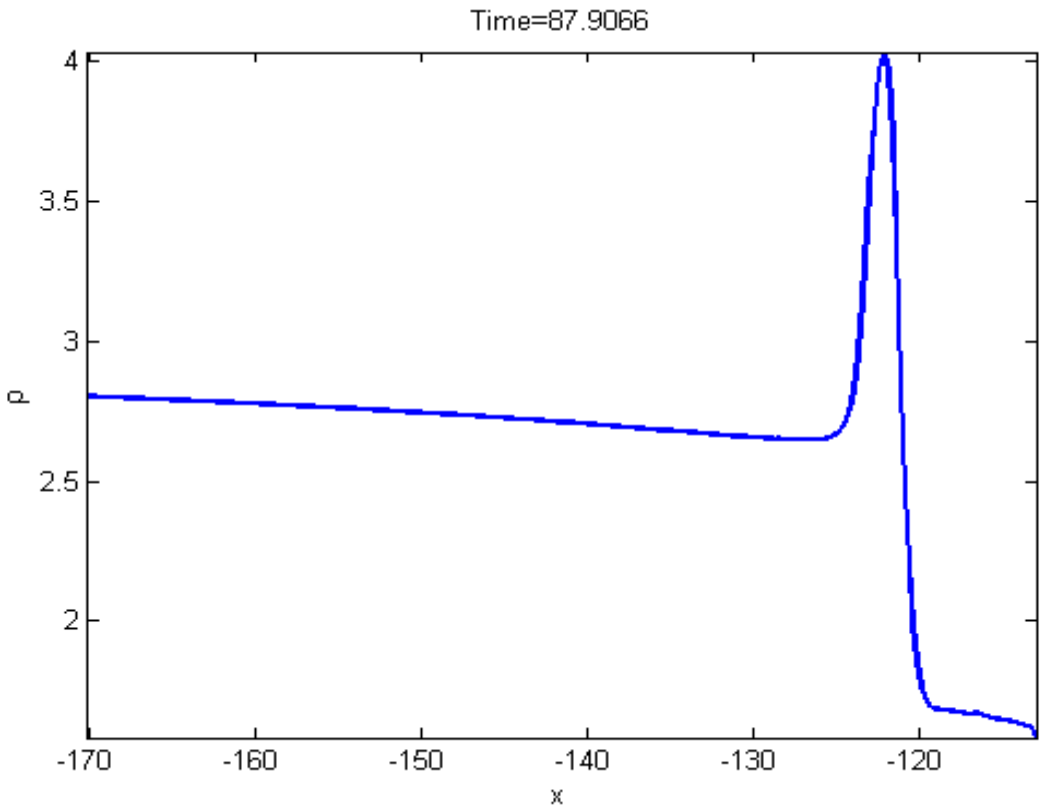

Figure 5.3: Density ρ obtained at different locations x in the transmitted shock region when $t = 87.9$.

5.3 The Zeroth-Order Solution in the Expansion Fan Region

In the Riemann problem, due to the refracted wave formed, the domain is divided into 5 regions as shown in the figure 5.4. The refracted wave $i.e.,$ the expansion fan is considered as the small region of space between the leading edge and the trailing edge of the refracted wave.[2]The perturbations in regions (0) and (3) are assumed to be zero. The solution expanding towards right due to the reflected expansion fan is evaluated by solving the zeroth-order equation (33), adding the boundary conditions and differentiating them with respect to time. The solution is discretized in Chebyshev polynomials and solved to obtain the time dependent solution. The boundary conditions for the expansion fan region are studied in the following section.

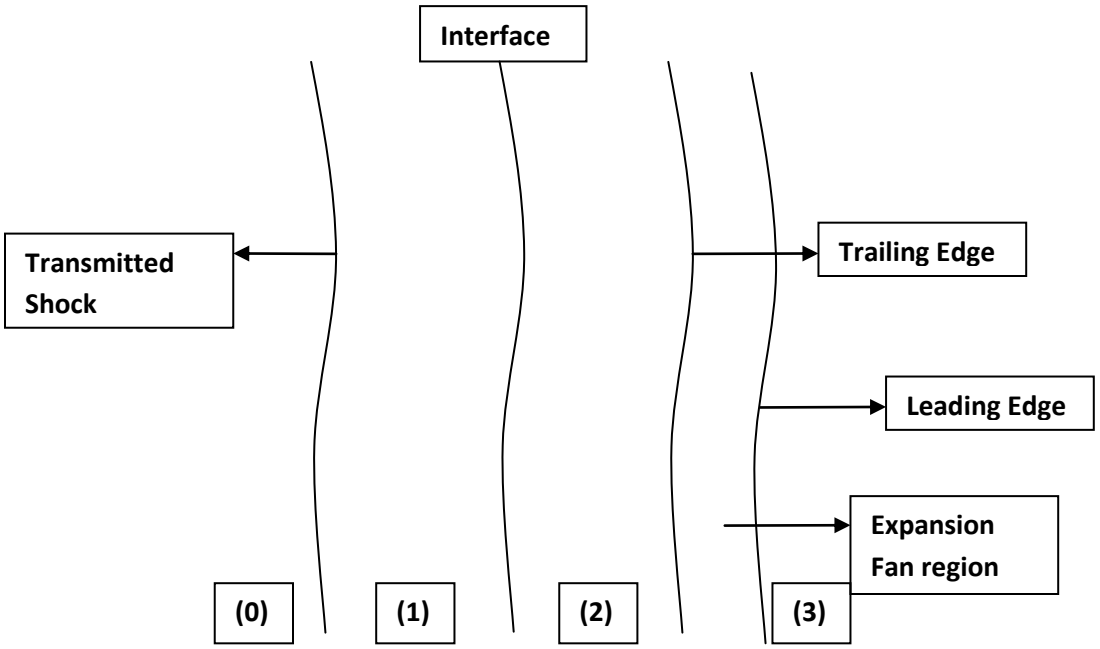

Figure 5.4: Figure showing the leading edge and the trailing edge of the expansion fan region.

The J^+ characteristics move towards right from interface at the expansion fan region and is given by

$$J^+ = uY + \frac{2}{\gamma - 1}a$$

where, uY is defined as the velocity at the interface and a is the speed of sound.The location of the leading edge in the expansion fan is given as

$$X_{LE} = X_0 + w_3 \Delta t$$

where, X_0 is the location of the interface, w_3 is the velocity of the expansion fan at region (3) in the figure 5.4 which is given as,

$$w_3 = u_3 + a_3$$

u_3 and a_3 are defined as the velocity and speed of sound at region (3), Δt is the difference in time period which is given by $\Delta t = t - t_0$. Also, t is the time period at different steps and t_0 is when $t = 0$.

Any specific point on the C^+ curve has a slope and is defined as

$$slope = \frac{1}{(uY + a)},$$

The location of the trailing edge of the refracted wave is given by the expression

$$X_{TE} = X_0 + \frac{t}{slope(1)},$$

$slope(1)$ is defined as the slope of the curve at the first time period. The location of the wave anywhere in space in the expansion fan region is given by the expression

$$\xi = X_0 + \frac{\vec{X} + 1}{2}(X_{LE} - X_0),$$

where, $\vec{X} = \cos\theta$ and $\theta \in (\pi, 0)$.

The C^- characteristic which moves towards left at region (3) is given as

$$J^-_3 = u_3 - \frac{2}{\gamma - 1}a_3.$$

From the method of characteristics if the values of J^+ and J^- are known at a given point, the local values of velocity u ,speed of sound a, pressure p, and density ρ are obtained with the following equations. Below are the equations for local values obtained when the location of shock is behind the trailing edge of the refracted wave.

$$u = \frac{1}{2}(J^+ + J^-_3),$$

$$a = \frac{\gamma - 1}{4}(J^+ - J^-_3),$$

$$p = p_3 * (a/a_3)^{(\frac{2*\gamma}{\gamma-1})},$$

$$\rho = (\frac{p}{p_3})^{1/\gamma} * \rho_3.$$

The above jump conditions are differentiated with respect to time and expanded in Chebyshev polynomials. The solutions for pressure, velocity and density obtained by solving the partial differential equation are as shown below.

Figure 5.5 shows the variation in pressure (p) at different locations $(x)$when $time = 87.9066$ in the expansion fan region. It is evident from the result that the pressure tends to decrease to the point where the trailing edge is formed and tends to increase with the formation of detonation wave.

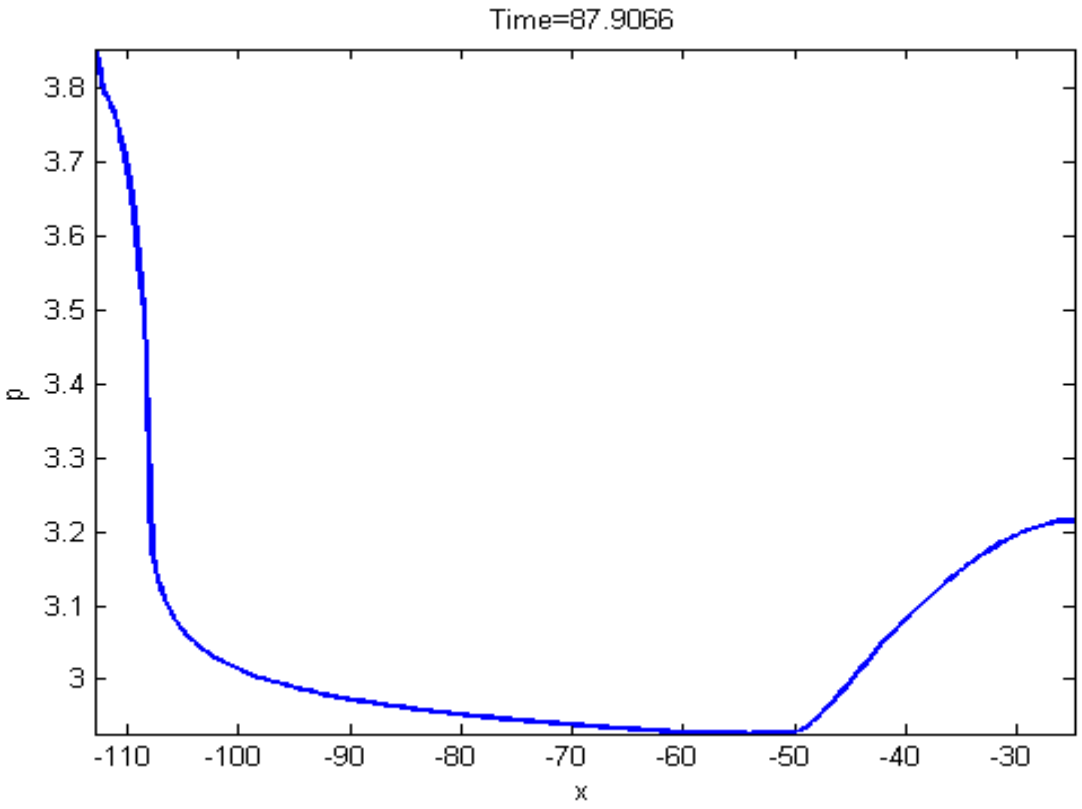

Figure 5.5: Plot showing the components of pressure p at different locations x obtained in expansion fan region when $t = 87.9$.

Figure 5.6 shows the components of velocity (u) at different locations (x) in the expansion fan region when $time = 87.9066$. There is a sharp decrease in velocity at the leading edge of the expansion fan. From the trailing edge of the expansion fan region, the velocity increases with the formation of detonation wave.

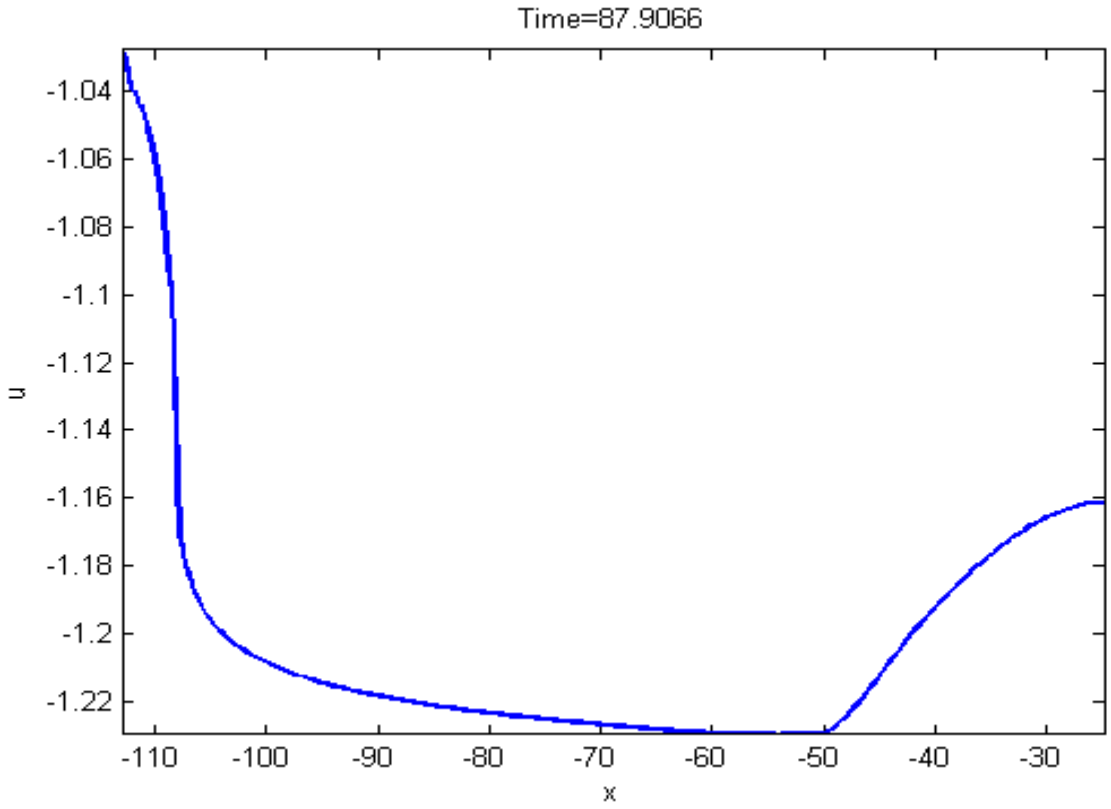

Figure 5.6: Plot showing the components of velocity u at different locations x obtained in expansion fan region when $t = 87.9$.

Figure 5.7 shows the components of density ρ at different locations x in the expansion fan region. The density in the expansion fan region tends to decrease from the leading edge of the expansion fan. At the trailing edge, the density tends to increase with the formation of a detonation wave.

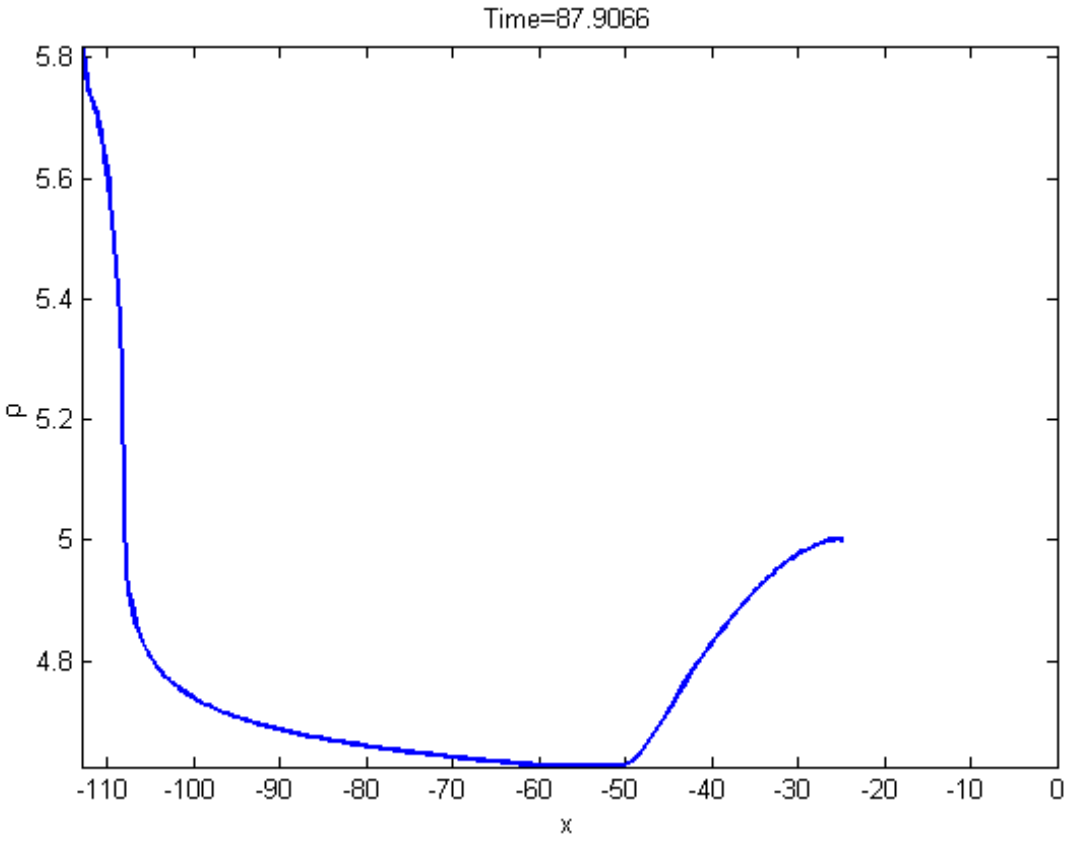

Figure 5.7: Plot showing the components of density ρ at different locations x obtained in expansion fan region when $t = 87.9$.

A graph is plotted which shows the location of each wave i.e. the transmitted shock wave, the interface the trailing and leading edge of the refracted shock wave at different time step as shown in the Figure 5.8.

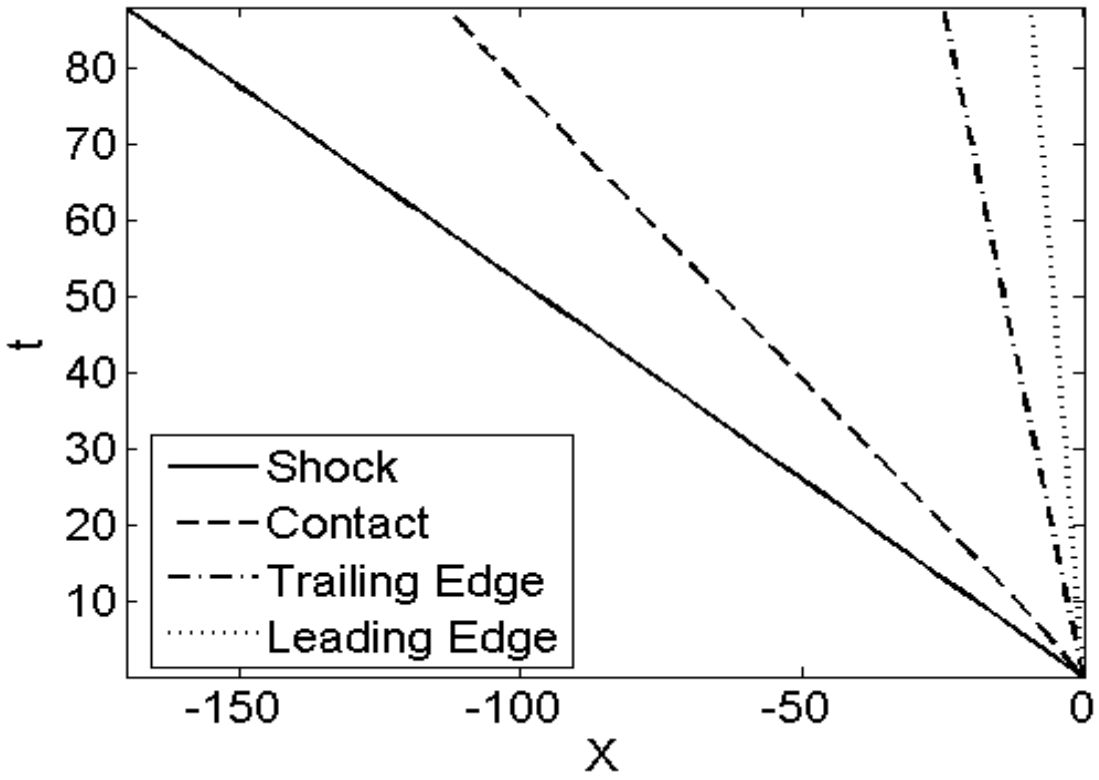

Figure 5.8: Plot showing the transmitted shock, contact interface, trailing and leading edge of the expansion fan region at different locations with respect to time.

CHAPTER 6

THE FIRST-ORDER PERTURBATION

6.1 Initial Values for First-Order Perturbation

The initial values of the interface perturbations, $a_j, j = 1..3$, are determined by the initial instantaneous acceleration imparted by the shock to the interface. These perturbations are normalized by the value at the contact discontinuity, $j = 2$, therefore,

$$a_j = \frac{1 - \frac{W_j}{W_{inc}}}{1 - \frac{W_2}{W_{inc}}},$$

The initial conditions in the above equation are similar to those reported by Richtmyer [1]. The conclusion that the initial compression of the interface is not affected by the reactivity is because the initial perturbation is assumed to be much smaller than the characteristic reaction length say, the half reaction distance. The non reactive RMI analysis is valid for $\epsilon k \ll 1$, where k is the interface disturbance wave number.

The remaining conditions for the first order perturbation are determined by taking the limit of equation (36) for $t = 0^+$, which corresponds with sending $\delta_0 \to 0$. The limit together with the boundary conditions yield a set of ordinary differential equations in ξ, which are solved using the same discretization as for the time dependent problem. Note that the previous result in equation (38) leads to $\lim_{t\to 0^+}(\frac{\partial P^1}{\partial \xi}) \neq 0$, and a non-zero initial perturbation. Physically the non-zero initial perturbation is explained by considering the passage of the incident shock through the initial perturbation. Fluid particles with different y intersect the interface at different times, leading to equation for a_j. When $\lim_{t\to 0^+}(\frac{\partial P^0}{\partial \xi})/\delta_0 \neq 0$, i.e., for reactive conditions, this yields an initial perturbation with constant but non-zero first derivative.

6.2 First-Order Perturbation

The time derivative of the perturbation at $t = 0$ is found by applying the L' Hospital's rule to the limit of equation (36) for $t = 0^+$. The resulting ordinary differential is similar in structure to equation (37), and requires boundary conditions for the time derivative of the first order perturbation, which are obtained by time differentiating the perturbation of the shock jump conditions.

6.3 Discretization

Equations (32) and (36) are discretized in the x direction using the Chebyshev tau method [9]. The time integration is carried out using a variable step stiff ODE solver, with maximum absolute tolerance set to 10^{-8}. A second-order A-stable time integrator has been used to advance the solution in time.

The solution domain is considered in two regions, marked as (1) and (2) in figure 8(b). In each region 135 Chebyshev polynomials are used to obtain the solution.

CHAPTER 7

RESULTS AND DISCUSSION

From the results obtained in validation problems, we can say that the Chebyshev-tau method is accurate for the model problems. In this problem, for a given heat release $Q = 10$ and the activation energy $E = 20$, the zeroth-order solution is discretized and solved as discussed in the section (6.3) to obtain the components of pressure, velocity, and density as shown in Figures 5.1-5.3 for the transmitted shock region.

Figure 5.1 shows that the pressure tends to increase and eventually decrease at the point where the detonation wave is formed and as the time progresses it becomes constant. Figure 5.2 depicts that the velocity in the transmitted shock region tends to decrease to a point where the detonation wave is formed, increases and becomes constant. Figure 5.3 shows the density in the transmitted shock region increases as the shock travels from high density region to low density region, decreases and eventually becomes constant. The components of pressure, velocity and density are obtained for the expansion fan region and are shown in Figures 5.5-5.7. Figure 5.5 shows that the pressure tends to decrease to the point where the trailing edge is formed and gradually increases with the formation of detonation wave. Figure 5.6 shows that there is a sharp decrease in velocity at the leading edge and from the trailing edge, the velocity increases with the formation of the detonation wave. Similarly, Figure 5.7 shows that the components of density tend to decrease from the leading edge of the expansion fan and increases from the trailing edge with the formation of the detonation wave.

The zeroth-order solution is used as the base flow for the first-order perturbation. Two graphs are plotted showing the corrugation of the contact interface and the transmitted shock wave as shown in the Figures 7.1-7.6. These are plotted at different time steps and taking different values for the wave number k say, ($k = 0.5, 1, \text{ and } 2$).

There is large influence of the wave number on the perturbation growth of the contact interface and also the transmitted shock wave. Figure 7.7 shows that there is a super linear growth in the amplitude of the contact interface and the transmitted shock wave corrugation, when the wave number is increased gradually from $0.5 - 2$.Figure 7.8 shows that the increase in wave number contributes to an increase in the deformation rate of the transmitted shock wave. The end time for the simulations is set to 25.

There is a small variation in the magnitude of the initial perturbation with the increase in heat release (Q) as shown in the figures 7.9-7.10. The amplitude of contact corrugation of the interface and transmitted shock decreases with the increase in non dimensional activation energy (E). Hence the value of E is taken as 20 and the computations are made for different heat release say $Q = 10, 15 \text{ and } 25$. The end time of the computations for Q=10, 15 and 25 are different for each value of Q, and is stopped for t<25. This is because the solution tends to become unstable. We thus summarize the results of the deformation growth rate analysis by noticing that the larger the initial perturbation wave number the larger is the instability. Also, the increase in heat release accounts to a significant growth in the deformation rate of the transmitted shock, which makes the flow become unstable.

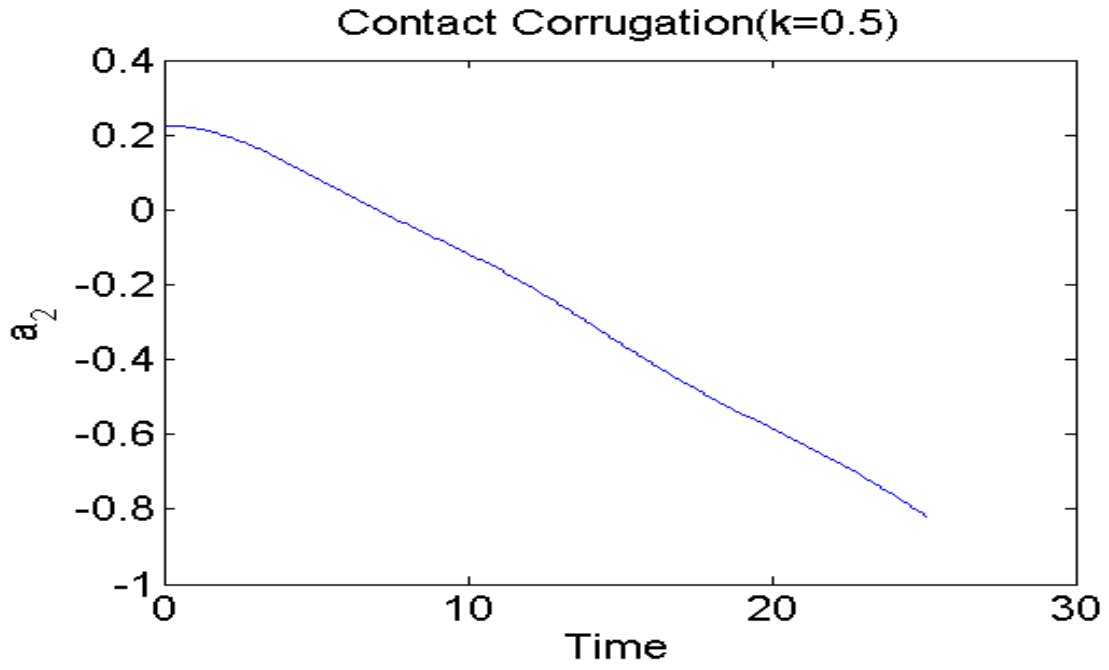

Figure 7.1: Plot showing the corrugation defined for contact interface at different time steps for $k = 0.5$.

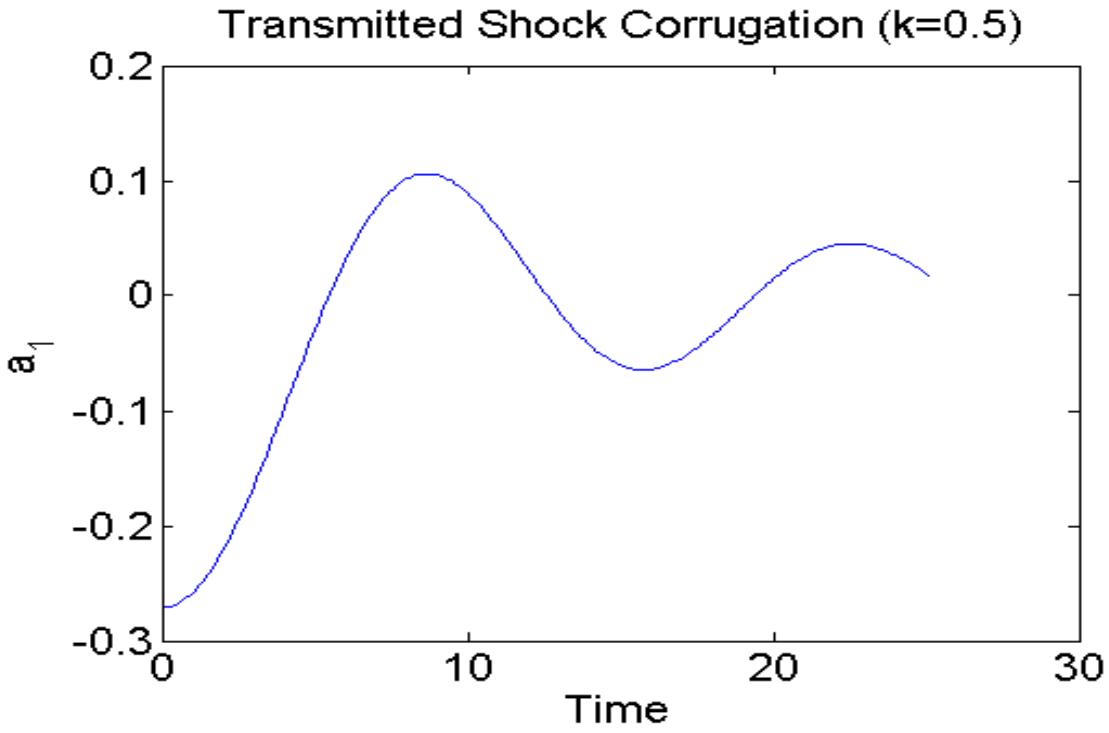

Figure 7.2: Plot showing the corrugation defined for transmitted shock wave at different time steps for $k = 0.5$.

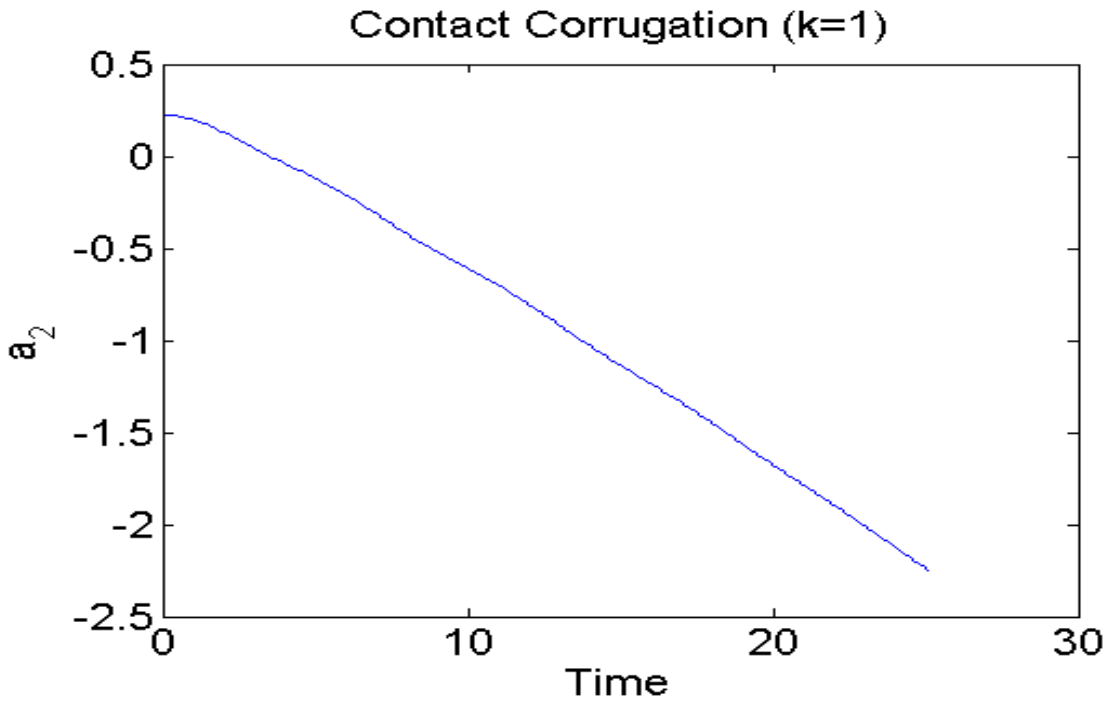

Figure 7.3: Plot showing the corrugation defined for contact interface at different time steps for $k = 1$.

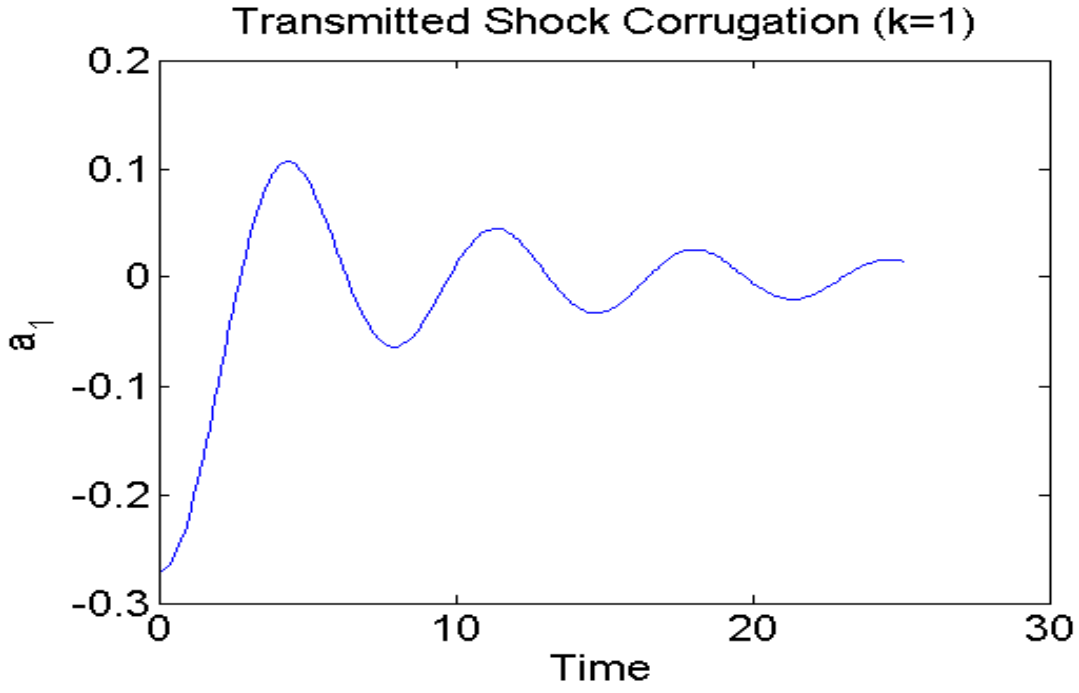

Figure 7.4: Plot showing the corrugation defined for transmitted shock wave at different time steps for $k = 1$.

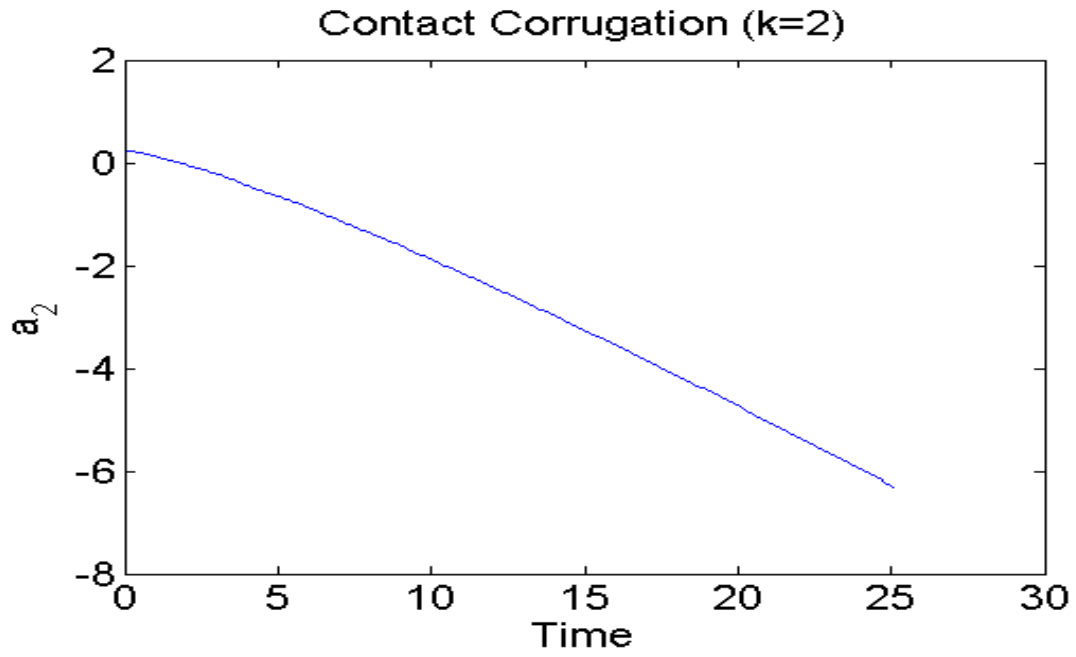

Figure 7.5: Plot showing the corrugation defined for contact interface at different time steps for $k = 2$.

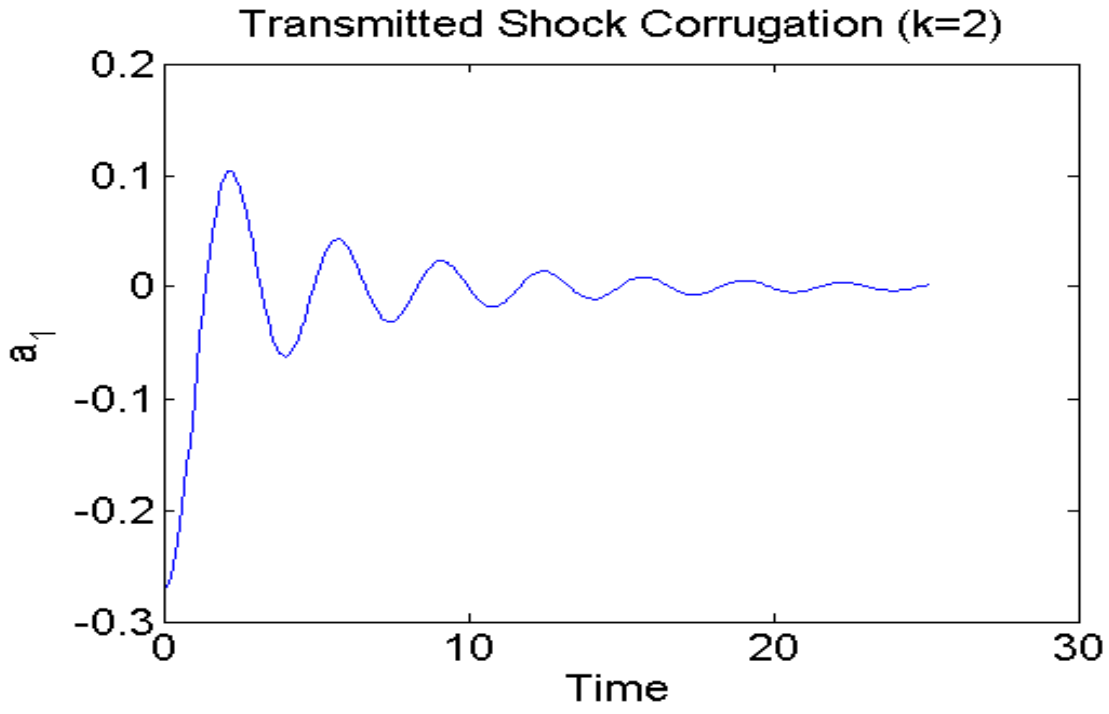

Figure 7.6: Plot showing the corrugation defined for transmitted shock wave at different time steps for $k = 2$.

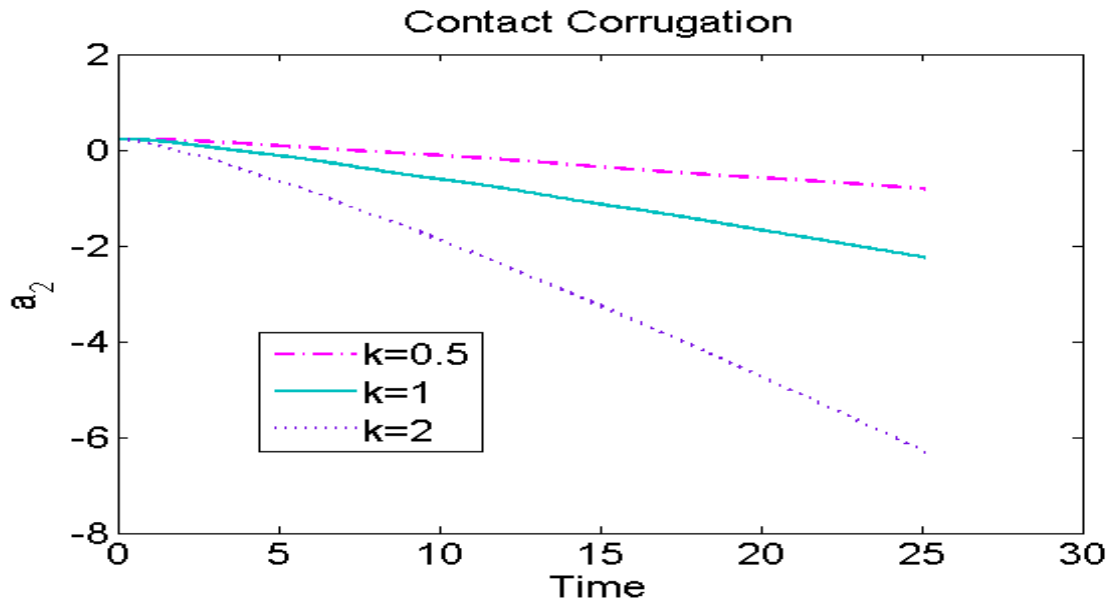

Figure 7.7: Plot showing the contact corrugation for three values of wave length k at different time steps. $k = 0.5$ is indicated with dash dot line, $k = 1$ is indicated by a solid line, $k = 2$ is indicated by a dotted line.

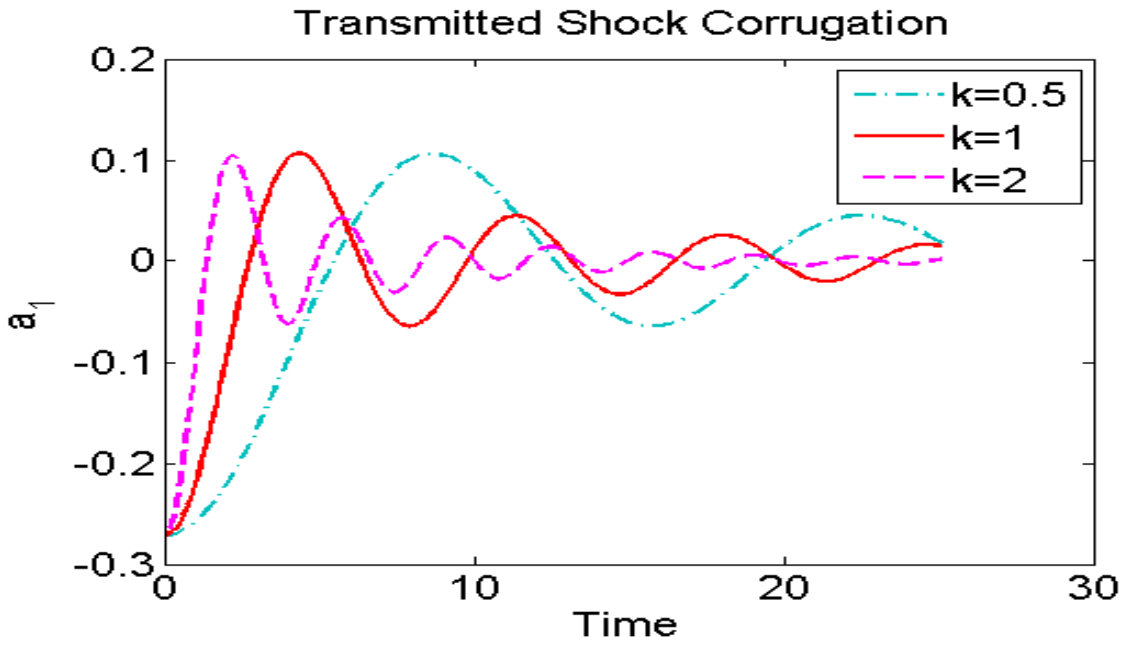

Figure 7.8: Plot showing the transmitted shock corrugation for three values of wave length k at different time steps. $k = 0.5$ is indicated with dash dot line, $k = 1$ is indicated by a solid line, $k = 2$ is indicated by a dotted line.

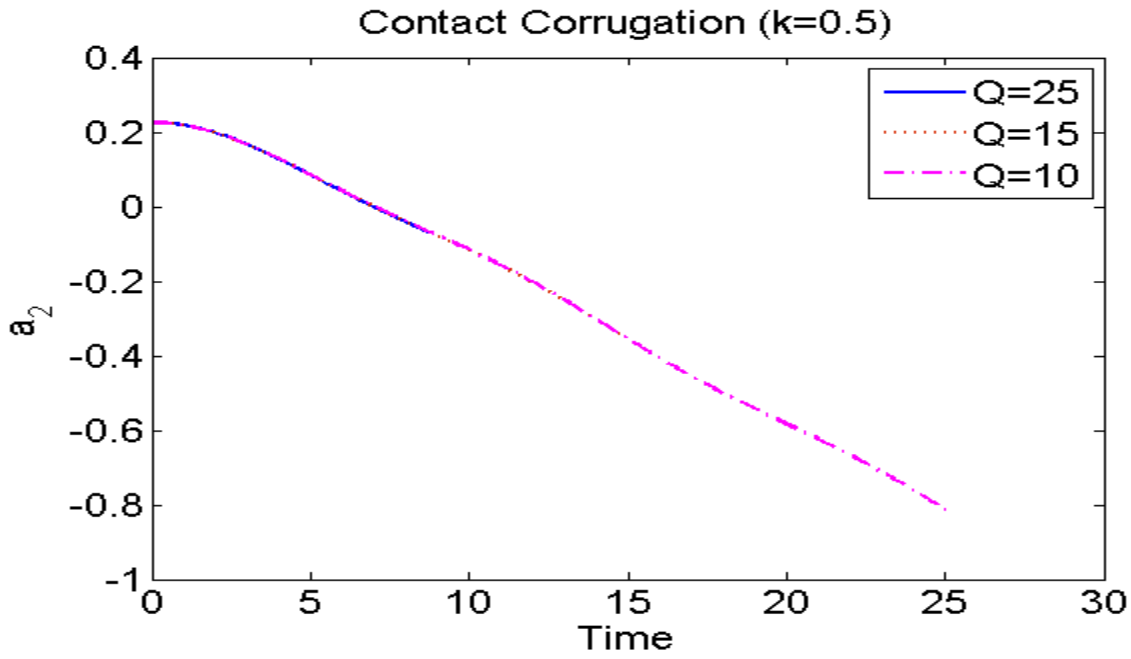

Figure 7.9: Plot showing the contact corrugation for three values of heat release Q at different time steps. $Q = 25$ is indicated by a solid line, $Q = 15$ is indicated by a dotted line, and $Q = 10$ is indicated with a dash dot line.

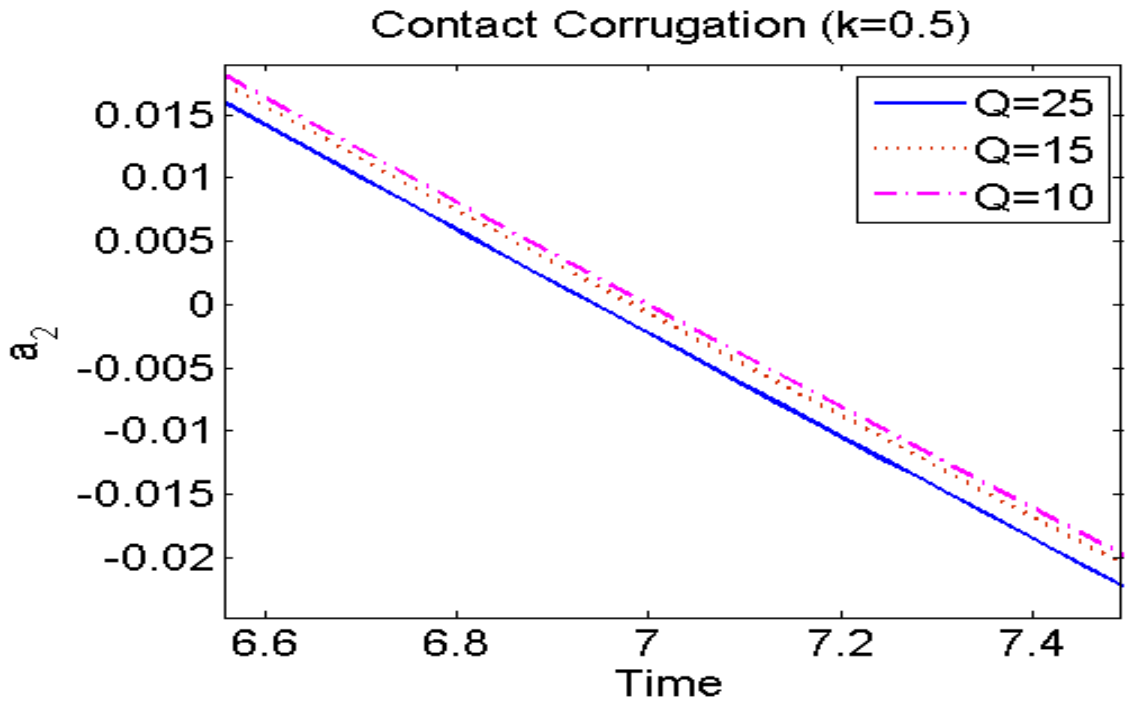

Figure 7.10: Plot showing the variation in the corrugation of the contact interface for different values of heat release.

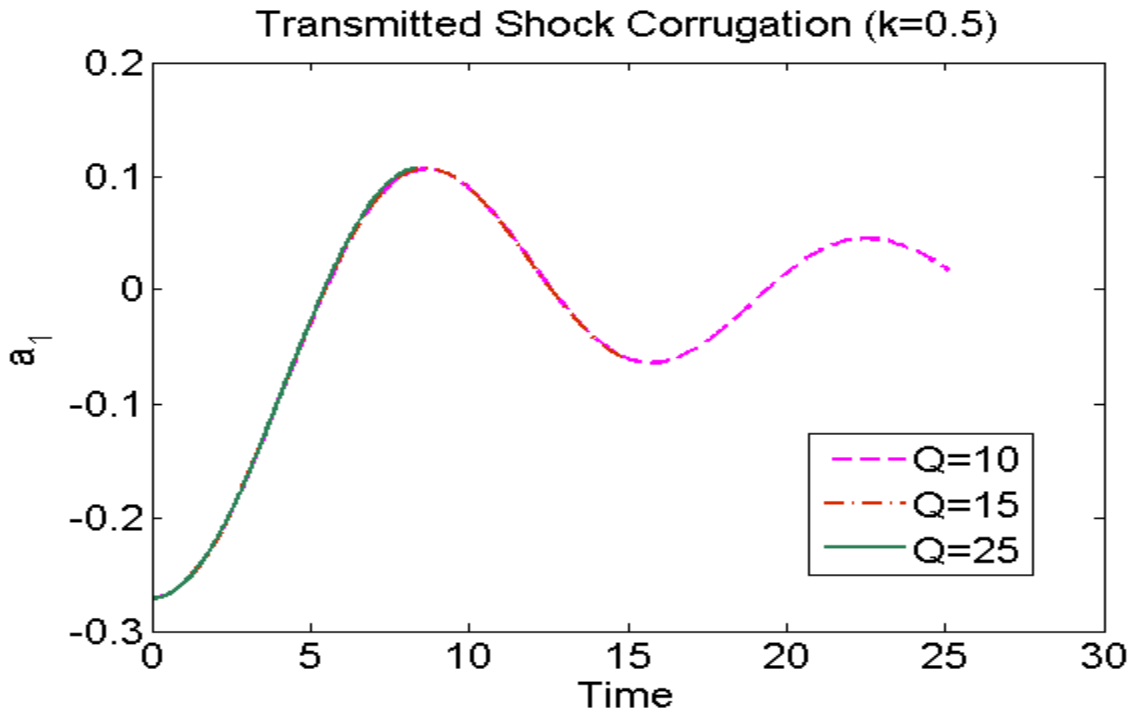

Figure 7.11: Plot showing the transmitted shock corrugation for three values of heat release Q at different time steps. $Q = 10$ is indicated by a dash line, $Q = 15$ is indicated by a dash dot line, and $Q = 25$ is indicated with a solid line.

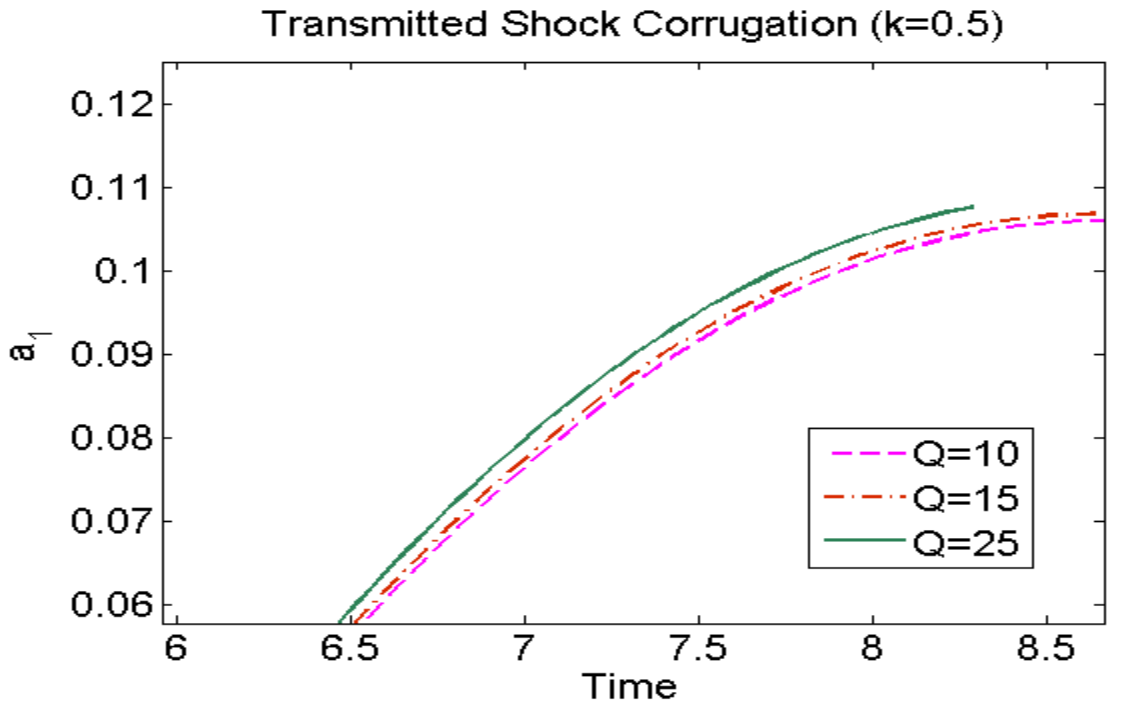

Figure 7.12: Plot showing the variation in the corrugation of the transmitted shock for different values of heat release.

CHAPTER 8

CONCLUSION AND FUTURE WORK RECOMMENDED

8.1 Conclusion

In this research we have analyzed the effect of reactivity in conjunction with the Richtmyer-Meshkov instability. The main conclusions we can draw from the results are:

1. The flow is destabilized by the interaction of shockwave with the perturbed interface, while the shocks remain stable.
2. The heavy-light fluid configuration with the passage of shock supports surface inversion, and hence the corrugation a_{-2} becomes negative as shown in the figure 7.7.
3. The increase in the wave number leads to a destabilization of the interface which is justified by the x/t similarity of the Euler equations.
4. Super-linear growth of interface is observed with the increase in the wavelength. This increase of wavelength tends to destabilize the flow and detonate the mixture.
5. A small growth in amplitude of the corrugations is observed in the transmitted shock and contact interface by increasing the heat release which allows the flow to become unstable.

8.2 Future Work Recommended

The present problem is solved assuming simple kinetics in the linear flow regime. Future work can include the analysis of detailed chemistry effects and the non-linear evolution of the surface. Detailed kinetics will provide a more realistic physical description of the problem, while non-linear analysis will shed light on the large time behavior of the reactive RMI.

REFERENCES

[1] Meshkov, Rictmyer., "*Taylor instability in shock acceleration of compressible fluids,"* Comm. Pure Appl. Math. XIII:297, (1960).

[2] Yang, Yumin., and Zhang, Qiang., "*Small amplitude theory of Richtmyer-Meshkov Instability,*" Phys. Fluids 6 (5), May (1994)

[3] Brouillette, Martin., and Sturtevant, B., *"Experiments on the Richtmyer-Meshkov instability: Small-scale perturbations on a plane interface,"* Phys. Fluids A, Vol. 5, No. 4, April (1993).

[4] Lindl, D., and Mead, W. C., "*Two-dimensional simulation of fluid instabilities in laser fusion pellets."* Phys. Rev. Lett. 34, 1273, (1975).

[5] Arnett D., *"The role of mixing in astrophysics."* Ap. J. Suppl. 127:213–17, (2000).

[6] Khokhlov., Oran., and Thomas. "*Numerical simulation of deflagration to detonation transition: The role of Shock-Flame interaction in turbulent flames."* Combust. Flame 117:323, (1999).

[7] Massa. L., and Lu, F.K., *"Role of the induction zone on turbulence-detonation interaction,"* Physics of fluids under review, (2008).

[8] Tomkins., Kumar., Orlicz., and Prestridge. *"An experimental investigation of mixing mechanism in shock accelerated flow."* J. Fluid Mech. 611:131, (2008).

[9] Dongarra., Straughan., and Walker., *"Chebyshev tau-QZ algorithm methods for calculating spectra of hydrodynamic stability problems."* Appl. Num. Math. 22:399, (1996).

[10] Khater, A.H., Temsah, R.S., Hassan, M.M., "*A Chebyshev spectral collocation method for solving Burgers'-type equations."* Journal of Computational and Applied Mathematics 222 (2008) 333–350, (2007)

BIOGRAPHICAL INFORMATION

Madhuri Ungarala was born in Hyderabad, Andhra Pradesh, India, in 1987. She received her Bachelor's degree in Aerospace Engineering from Jawaharlal Nehru Technological University, Hyderabad, India, in 2008. She joined University of Texas at Arlington to pursue her graduate studies in Aerospace Engineering in the year 2008. Her research interests include Gas Dynamics, Hypersonic Combustions and Detonations, and Programming in MATLAB.